Dynamic Instability of Microtubules: Monte Carlo Simulation and Application to Different Types of Microtubule Lattice

Stephen R. Martin,* Maria J. Schilstra,‡ and Peter M. Bayley*
*Division of Physical Biochemistry, National Institute for Medical Research, Mill Hill, London, England; ‡Department of Bio-organic Chemistry, Bijvoet Center for Bio-Molecular Research, University of Utrecht, Utrecht, the Netherlands

ABSTRACT *Dynamic instability* is the term used to describe the transition of an individual microtubule, apparently at random, between extended periods of slow growth and brief periods of rapid shortening. The typical sawtooth growth and shortening transition behavior has been successfully simulated numerically for the 13-protofilament microtubule A-lattice by a lateral cap model (Bayley, P. M., M. J. Schilstra, and S. R. Martin. 1990. *J. Cell Sci.* 95:33–48). This kinetic model is now extended systematically to other related lattice geometries, namely the 13-protofilament B-lattice and the 14-protofilament A-lattice, which contain structural "seams." The treatment requires the assignment of the free energies of specific protein-protein interactions in terms of the basic microtubule lattice. It is seen that dynamic instability is not restricted to the helically symmetric 13-protofilament A-lattice but is potentially a feature of all A- and B-lattices, irrespective of protofilament number. The advantages of this general energetic approach are that it allows a consistent treatment to be made for both ends of any microtubule lattice. Important features are the predominance of longitudinal interactions between tubulin molecules within the same protofilament and the implication of a relatively favorable interaction of tubulin-GDP with the growing microtubule end. For the three lattices specifically considered, the treatment predicts the dependence of the transition behavior upon tubulin concentration as a cooperative process, in good agreement with recent experimental observations. The model rationalizes the dynamic properties in terms of a metastable microtubule lattice of tubulin-GDP, stabilized by the kinetic process of tubulin-GTP addition. It provides a quantitative basis for the consideration of in vitro microtubule behavior under both steady-state and non-steady-state conditions, for comparison with experimental data on the dilution-induced disassembly of microtubules. Similarly, the effects of small tubulin-binding molecules such as GDP and nonhydrolyzable GTP analogues are readily treated. An extension of the model allows a detailed quantitative examination of possible modes of substoichiometric action of a number of antimitotic drugs relevant to cancer chemotherapy.

1. INTRODUCTION

Dynamic instability is the term given to the behavior of an individual microtubule, which interconverts, apparently at random, between extended periods of slow growth and brief periods of rapid shortening. Deduced originally from observations of length redistribution in microtubule populations (1, 2), it has since been established and quantified by direct real-time microscopic observations (3–5). Several reviews of microtubule dynamics have appeared recently (6–12).

A numerical kinetic model has been developed that simulates the main experimental observations of length changes, frequencies of switching between states, and utilization of GTP in tubulin assembly for either end of the 13-protofilament microtubule A-lattice (7, 13–16). In contrast to previous mechanisms (e.g., Ref. 17), this *lateral cap model* is characterized by the restriction of Tu-GTP to the terminal layer at the microtubule end, with the assembly-dependent GTP hydrolysis closely coupled to the addition of further Tu-GTP molecules. (These principles are reviewed in Ref. 10.)

Microtubules are known to exist with a range of values of the protofilament number, n. Those assembled from axonemes (18) or centrosomes (19) appear to retain the protofilament number of the nucleating structure, generally $n = 13$. For self-assembly in solution, microtubules with $n = 12$ to 17 have been observed, with $n = 13$ and 14 the most common (20). Also, Chrétien et al. (21) have observed changes in n (occurring rather infrequently) along an individual microtubule. Thus, uniqueness or constancy of protofilament number in dynamic instability cannot be assumed. In addition, microtubule lattices that differ in the arrangement of the tubulin monomer have been proposed (i.e., A-type and B-type) (22). All lattices, other than A-type ones with odd values of n, must contain mixed A- and B-type interactions (23, 24) giving rise to a longitudinal structural discontinuity. Song and Mandelkow (25) have recently presented evidence supporting the B-type microtubule lattice for several different tubulin structures.

The ability of the lateral cap model to simulate the transition behavior characteristic of microtubule dynamic instability for the 13-protofilament microtubule A-lattice (14)

Received for publication 25 January 1993 and in final form 3 May 1993.

Address reprint requests to Dr. Peter M. Bayley, Division of Physical Biochemistry, National Institute for Medical Research, The Ridgeway, Mill Hill, London NW7 1AA, England.

Abbreviations used: Tu-GTP, tubulin-GTP, tubulin $\alpha\beta$ heterodimer with GTP at the exchangeable nucleotide binding site; Tu-GDP, tubulin-GDP, tubulin $\alpha\beta$ heterodimer with GDP at the exchangeable nucleotide binding site; 13-A, 13-B, 14-A, microtubule lattices of A- or B-type with 13 or 14 protofilaments; MAPs, microtubule-associated proteins; n, microtubule protofilament number.

0006-3495/93/08/578/19 $2.00

raises the question of how these dynamic properties might be predicted to vary with different lattice types. In order to generalize the lateral cap model we have now developed a systematic treatment in terms of lattice interaction energies (cf. the treatment for actin filaments, Ref. 26) that can be applied to these different geometries. To develop this general method for treating all lattices, irrespective of type (A, B, or mixed A and B) and protofilament number (n), association constants (and therefore kinetic constants) must be defined for all possible binding sites, in which both the configuration of neighboring subunits and their nucleotide content may vary. Therefore, one needs to consider all of the formal interactions of a given tubulin $\alpha\beta$ heterodimer with its immediate neighbors in the lattice.

Using a small number of reasonable assumptions we show that all microtubule lattices can be treated in a consistent way. The main result is that the property of microtubule dynamic instability is not restricted to the helically symmetric 13-protofilament A-lattice but is potentially a property of any microtubule lattice type. The treatment is readily extended to simulate the dynamic behavior of microtubules under a wide variety of conditions accessible to experimentation. These include disassembly induced by rapid dilution and the effects of Tu-GDP, anti-mitotic drugs, and nonhydrolyzable analogues of GTP. Tu-GDP and anti-mitotic drugs such as colchicine and podophyllotoxin are predicted to exert significant effects on microtubule dynamics. These results indicate that specific ligands binding selectively to tubulin can, in principle, exercise sensitive control over the properties of microtubule arrays within a cellular environment. This regulatory characteristic can be understood in terms of its effect upon the unique physical properties of the microtubule lattice structure.

2. DEFINITION OF THE MODEL

2.1. The Lateral Cap Model

Microtubule growth is most simply formulated as the reversible addition of a single molecule of tubulin-GTP to the end of a microtubule containing x molecules, elongating the lattice by a single molecule:

$$(\mathrm{MT})_x + \text{Tu-GTP} \; (\mathrm{MT})_{x+1}$$

Microtubule shortening is likewise most simply formulated as the loss of a single molecule of tubulin-GDP from the end of a microtubule containing x molecules, decreasing the lattice by a single molecule in a process usually considered to be irreversible.

$$(\mathrm{MT})_x \rightarrow (\mathrm{MT})_{x-1} + \text{Tu-GDP}$$

At a certain (critical) concentration of Tu-GTP, a steady state is reached in which growth and shortening processes are balanced, and, given an adequate supply of GTP, the microtubule polymer mass remains constant. The addition of one molecule of Tu-GTP to the microtubule lattice is accompanied by the hydrolysis of one molecule of GTP (27). The exact temporal and spatial relationships between tubulin addition and GTP hydrolysis are not known. Hence, the chemical species (Tu-GTP, Tu-GDP, or an intermediate) present at the microtubule end cannot be defined unambiguously. The experimental evidence for the composition of the microtubule end has been discussed recently (see above references to reviews). At steady state, the amount of Tu-GTP present at the microtubule end is at or less than the limit of analytical detection.

The lateral cap model for microtubule dynamics seeks to represent this dynamic system in terms of the simplest possible structure and the minimum number of kinetic parameters. The main postulates of the formulation (7, 13, 14, 16) are as follows:

(a) The affinity of Tu-GTP for a particular site at the end of the microtubule is highest when the Tu-GTP content of the site is high. This reflects the experimental observation of the requirement for Tu-GTP rather than Tu-GDP for microtubule assembly, and the inherent instability of a lattice comprising entirely Tu-GDP.

(b) The addition of Tu-GTP is coupled to the hydrolysis of one molecule of GTP in the β-subunit of a previously terminal Tu-GTP molecule. Tubulin-GTP is thus restricted to terminal positions, where it comprises a lateral cap, and the bulk of the microtubule then contains only Tu-GDP.

The microtubule elongation reaction can then be formally written as

$$(\mathrm{MT})_x(\text{Tu-GTP})_y + \text{Tu-GTP} \rightarrow (\mathrm{MT})_{x+1}(\text{Tu-GTP})_y + \mathrm{P}_i$$

where $(\mathrm{MT})_x$ represents a microtubule lattice comprising x Tu-GDP molecules, and $(\text{Tu-GTP})_y$ represents a terminal layer of y molecules of Tu-GTP. The net reaction is the extension of the lattice by one molecule of Tu-GDP and the hydrolysis of one molecule of GTP.

2.2. Microtubule lattices

Fig. 1 shows a schematic representation of the 13-protofilament A-type lattice. Fig. 1 *A–C* shows different configurations of the microtubule end in the growing state (G), with a lateral cap of 13 Tu-GTP molecules in the terminal position of each of 13 protofilaments. The postulate of coupled hydrolysis is illustrated in the addition reactions 1A→1B→1C. Fig. 1 *D–F* shows the loss of successive molecules of Tu-GTP from the lateral cap of Fig. 1 *B*, leading eventually to the configuration 1F with Tu-GDP exclusively in terminal positions, characteristic of the shortening state (S). The behavior of the microtubule end is simulated as a stochastic process of such individual addition and dissociation steps, which produces an essentially two-state behavior of growth (G) and shortening (S) with transitions G→S and S→G as discussed below. Structures 1D and 1E represent configurations with "mixed ends"; these are typical minority species that are kinetic intermediates between states G and S.

Microtubule lattices may be defined in general in terms of their protofilament number (n = 13, 14, etc.) and their helical symmetry. All microtubule lattices appear similar at the level of the tubulin monomer (i.e., ignoring α, β differences) in

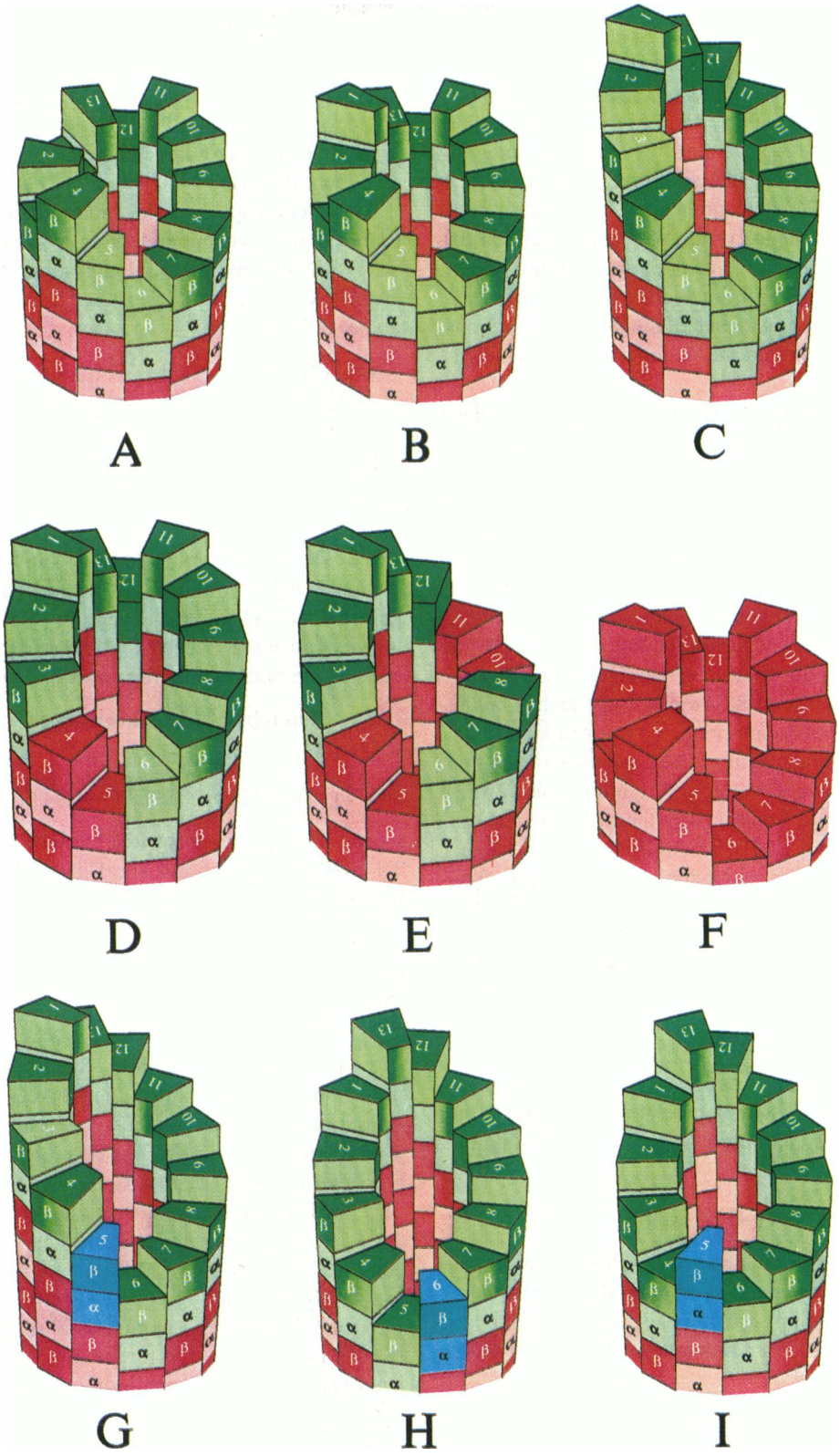

FIGURE 1 Illustration of the lateral cap model for microtubule dynamic instability. Dark green, β-tubulin-GTP; dark red, β-tubulin-GDP; light green and light red, α-tubulin. The microtubule is shown (not to scale) as a 13-protofilament A-type lattice, to illustrate the relative positions of the α- and β-subunits, depicted schematically as volume-filling elements. (*A–C*) The growing microtubule. The single molecule of Tu-GTP (*green*) at the end of each protofilament comprises a terminal layer, or lateral cap, the configuration of which determines the number of equivalent association (or dissociation) sites. In (*A*), these occur on protofilaments 1,3,6,12 (and 2,4,11,13). In (*B*), the addition of one molecule to protofilament 1 gives a configuration with binding sites on protofilaments 3,6,12 (and dissociation sites on protofilaments 1,4,11). In (*C*), additions to protofilaments 3,2,12,13,1 give the configuration with one association site (protofilament 6) and one dissociation site (protofilament 13). In this model, the addition of a molecule of Tu-GTP is coupled to the hydrolysis of the previously terminal Tu-GTP in the same protofilament, thus conserving the single layer cap: compare protofilaments 1,2,3,12,13 in (*B*) and (*C*). (*D–F*)

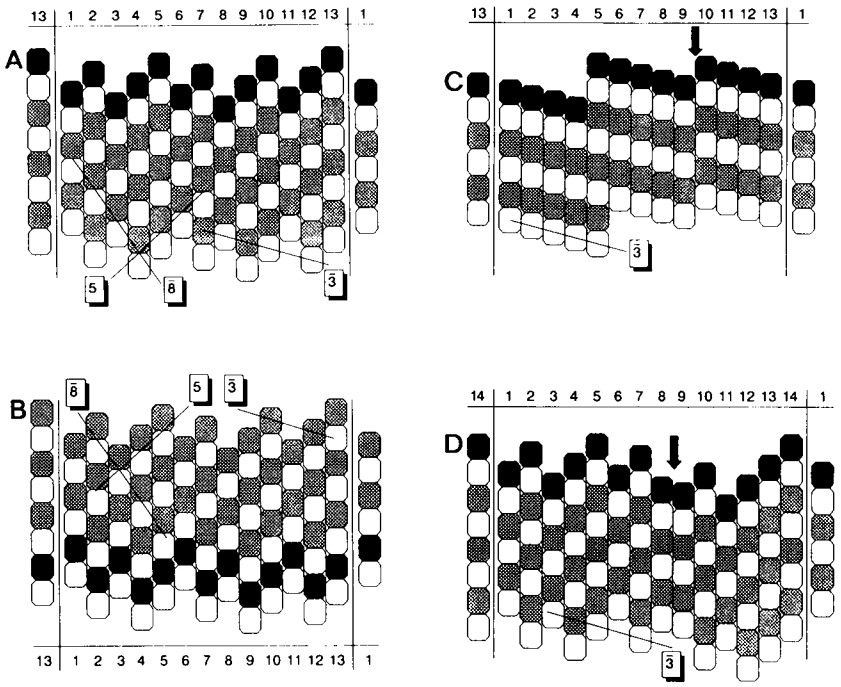

FIGURE 2 Microtubule lattices shown in planar projection. (*A*) The β-out end of the 13-protofilament A-lattice. (*B*) The α-out end of the 13-protofilament A-lattice. (*C*) The β-out end of the 13 protofilament B-lattice; the seam is arbitrarily positioned between protofilaments 9 and 10. (*D*) The β-out end of the 14 protofilament A-lattice; the seam is arbitrarily positioned between protofilaments 8 and 9. The left-handed $\bar{3}$-start monomer helix and the 5-start right-handed and $\bar{8}$-start left-handed dimer helices are indicated where appropriate. Tubulin monomers are identified as α (*light shading*), β containing GTP (black), and β containing GDP (*cross-hatched*).

that they possess a family of three left-handed helices (22). In the 13-protofilament A-lattice the αβ heterodimers are arranged as shown in Fig. 2 (*A* and *B*) with heterologous α-β and β-α contacts along the $\bar{3}$-start helix (the bar indicates left-handedness). In addition to the $\bar{3}$-start monomer helix this structure is seen to contain 5-start and $\bar{8}$-start dimer helices; the dimer lattice is therefore helically symmetric. In the 13-protofilament B-lattice the αβ heterodimers are arranged as shown in Fig. 2 *C*, with homologous α-α and β-β contacts along the $\bar{3}$-start helix. This dimer packing arrangement means that the 13-protofilament B-lattice must contain a discontinuity or "seam" with heterologous α-β and β-α contacts (23, 24). Thus, the 5- and $\bar{3}$-start dimer helices are not present in this lattice type.

All B-type lattices have a seam, irrespective of the number of protofilaments; all A-type lattices with even numbers of protofilaments (n = 14, 16, etc.) also have a seam and thus also lack perfect helical symmetry at the level of the tubulin αβ-heterodimer (23, 24). For example, inspection of the two-dimensional representation of the 14-protofilament microtubule A-lattice (Fig. 2 *D*) shows that it contains a seam of α-α and β-β contacts on the $\bar{3}$-start helix.

For microtubules with a protofilament number greater than 13 (irrespective of type, A or B), the lattice geometry must be different from that of the 13-protofilament lattices, in order to accommodate the extra protofilament while maintaining the $\bar{3}$-start monomer helix. This may occur either by slightly altering the lateral registration of adjacent protofilaments (24) or by retaining the same relationship of individual monomers but allowing a slight superhelical twist in the lattice. Evidence has been presented that favors the latter case, for example, for n = 14, a protofilament skew angle of ~0.8° is observed (20). In the two-dimensional representations of lattices used here we have, simply for convenience, accommodated the extra protofilament by a small alteration in the lateral registration of monomers.

Transition to the shortening microtubule. Starting from (*B*), loss of Tu-GTP from protofilaments 4 and 5 generates the microtubule with a "mixed end" of Tu-GTP and Tu-GDP shown in (*D*); similarly, subsequent loss from protofilaments 11,10,9 generates the configuration (*E*); loss from protofilaments 1,2,3,13,12 and 8,7,6 generates the configuration (*F*) in which the end is exclusively Tu-GDP (*red*) and completes the transition growing to shortening (G→S). This configuration (*F*) shows the typical condition for the optimal rate of shortening. (*Note:* All processes of association and dissociation of Tu-GTP are reversible; the reverse sequence F, E, D, B is one of many possible routes for the re-establishment of the lateral cap, via an S→G transition.) (*G–I*) Substoichiometric inhibition of microtubule dynamics by tubulin-drug complex. The tubulin-drug complex (Tu-X) is shown as blue. The Tu-X complex binds to the microtubule end at a single site but inhibits further addition reactions in the adjacent site. In (*G*), Tu-X at position 5 inhibits addition at the 5-start related position on protofilament 6; in (*H*), Tu-X at position 6 inhibits addition at the $\bar{8}$-start related position on protofilament 5; in (*I*), the Tu-X complex at position 5 inhibits addition at both the 5 and $\bar{8}$-start related sites. We describe these as type 1 inhibition (*G* and *H*) and type 2 inhibition (*I*). Addition reactions build up the lattice to the configuration shown, which has a single dissociation site at position 1 (in *G*) or 13 (in *H* and *I*). The only association sites are inhibited, and growth is arrested until an ordered series of dissociation events occurs (e.g., from protofilaments 1,2,3,4,5 in *G*), leading to the loss of the Tu-X complex, or (with low probability) the inhibited sites become occupied, the Tu-X complex is incorporated into the lattice, and growth continues. Because of the closed nature of the microtubule end, a single inhibitor complex acting at a concentration strongly substoichiometric to the C_c for assembly would suffice to arrest the growth of the whole microtubule (Ref. 45 and data presented at the Second Interface of Clinical and Laboratory Responses to Anti-Cancer Drugs, Marseille, April 1992).

In order to be able to treat microtubule lattice geometries with all possible interactions at the level of the tubulin monomer, we adopt a monomer numbering scheme illustrated, for both ends of the 13-protofilament A-lattice, in Fig. 3. In this scheme, z (= zero) identifies the terminal β-subunit of the protofilament under consideration. Other subunits are then identified in positions plus (p) and minus (m) relative to z, corresponding to the principal lattice directions. For the 13-protofilament B-lattice the numbering scheme is exactly the same as for the 13-A, but the α- and β-subunits are arranged differently (see Fig. 2 *C*). The introduction of an additional protofilament as in the 14-protofilament A-lattice (Fig. 2 *D*) requires a slightly different numbering scheme (see Fig. 3).

Interactions between monomers are specified using the notation ΔG_{Djk}, where D indicates the direction of the interaction; D = 3, 10, 13, or 16 in the case of the 13-protofilament lattices. In the case of the 13-protofilament A-lattice (only) the values of D = 10 and 16 correspond to the 5 and $\bar{8}$-start dimer helices (see above). The indices j and k specify the nature of the monomers involved in the interaction, and these may be α (α-subunit), d (β-subunit with GDP at the E-site), or t (β-subunit with GTP at the E-site). For example, $\Delta G_{3\alpha t}$ is the free energy of interaction between an α-subunit and a GTP-containing β-subunit along the $\bar{3}$-start helix. The index j always refers to the subunit in position ($+D$) relative to the position of the subunit identified with index k.

2.3. The computational procedure

The steps involved in the Monte Carlo simulation of one end of a microtubule at a fixed external concentration of Tu-GTP ([Tu-GTP]) are as follows:

STEP 1. Examine the end of each protofilament in the microtubule to see if it is part of a site for dissociation and/or association. The total number of sites to be considered, i, is the number of sites for association plus the number of sites for dissociation.

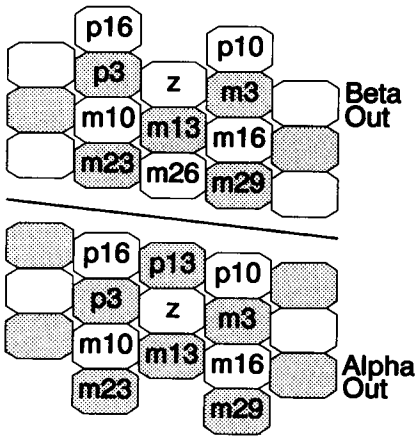

FIGURE 3 The monomer numbering scheme used in the simulations, illustrated for both ends of the 13-A lattice. The terminal β-subunit of the molecule under consideration is identified by *z* (= zero). Other subunits are numbered as plus (*p*) and minus (*m*) relative to this position. The α-subunits are lightly shaded, and the β- subunits are unshaded. For the 14-filament A-lattice the numbering scheme is modified to accommodate the extra protofilament. Thus, p10 becomes p11, p16 becomes p17, m13 becomes m14, and so on.

STEP 2. For each of the total of i sites assign a rate constant, k_i, for a dissociation event ($k_i = k_i(-)$) and/or for an association event ($k_i = k_i(+) \cdot$ [Tu-GTP]). In general, the value of the rate constant is determined by the physical structure of the binding site and by the nucleotide content of the β-subunits in adjacent protofilaments (see Section 2.4).

STEP 3. For each site, i, calculate the time, t_i, at which the association or dissociation event would occur stochastically using the equation (28)

$$t_i = -\ln(1 - R_i)/k_i$$

where R_i is a uniformly distributed random number in the range 0 to 1.

STEP 4. Implement the event (either addition or dissociation of one molecule of tubulin) that has the smallest value of t_i (t_{min}) and modify the lattice at the end of the appropriate protofilament as follows:

(*a*) For any event, by adding Tu-GTP or removing either Tu-GTP or Tu-GDP, as appropriate.

(*b*) For an addition event, by allowing for GTP hydrolysis. In the work presented here we use (for both ends) a longitudinal Hydrolysis Rule, in which the GTP hydrolyzed is the previously terminal β-subunit of the same protofilament to which the incoming Tu-GTP molecule is added. (Other spatial relationships are considered in Ref. 16.)

STEP 5. Extend the total elapsed time for the simulation by t_{min} and repeat the calculation from Step 1.

The behavior of the single microtubule is simulated over a large number of events, and a plot of microtubule length versus time ($L(t)$) plot) is constructed. The net growth of the single microtubule over very long times simulates the net behavior of a microtubule population. Therefore, by performing such extended simulations at a number of different external Tu-GTP concentrations one can construct a plot of net growth rate versus [Tu-GTP] (the $J_{on}C$ plot). This gives the critical concentration (C_c) for the macroscopic system, defined as the concentration of Tu-GTP at which the net growth rate is zero. Examination of the $L(t)$ plot also allows one to estimate the mean lifetimes of the growing and shortening states (T_g, T_s), as well as individual rates of growth and shortening (R_g and R_s). Individual phases are defined as length excursions greater than 0.15 μm, and transition points are defined as the intersection of two such phases.

2.4. Definition of binding sites

The simulation treats a given microtubule lattice geometry (e.g., 13-A, 14-A, 13-B, etc.) in terms of the individual association and dissociation steps of single tubulin molecules, the kinetics of these steps being determined entirely by the composition of the association or dissociation site in terms

of neighboring Tu-GTP and/or Tu-GDP molecules. In previous work (and following the concept of Chen and Hill (17) for the 13-protofilament microtubule A-lattice), the site for association or dissociation was defined in terms of one specific geometric configuration of adjacent molecules. In the Chen and Hill formulation the addition of one Tu-GTP completed monomer interactions in the $\bar{3}$- and 10-start directions, as well as making a longitudinal (or 13-start) contact. In our modification (16) the site was defined differently; the addition reaction completed interactions in the $\bar{3}$-, 10-, and $\overline{16}$-start directions. This definition derived from a consideration of the minimum number of protein-protein contacts thought necessary to constitute a stable interaction with the microtubule end.

The typical site for an association reaction at a microtubule end is shown in Fig. 3. That is, a binding site for Tu-GTP at the β-out end of the central protofilament requires that positions p16 and p10 are occupied. An addition reaction may, but does not necessarily, create a new binding site (also see Fig. 4), so that the instantaneous number of binding sites at the microtubule end can fluctuate. For a 13-protofilament A-lattice the maximum number of sites for association is 5, with means of 3.82 (17) and 3.33 (16). The mean value is the time average of the instantaneous number of sites and reflects the changing end configuration—namely, how the runs of tubulin in the 5- and $\bar{8}$-start dimer directions are distributed around the closed cylindrical structure. The tubulin dimer designated {z/m13} is allowed to dissociate only if the dimers designated {p16/p3} and {p10/m3} are absent. This dissociation generates a new site for an association reaction. The situation at the α-out end is exactly analogous.

With this "fixed geometry" site we distinguish between binding sites on the microtubule end solely in terms of the nucleotide content (either GTP or GDP) at the β-subunit of tubulin dimers in adjacent protofilaments (see Fig. 4). Therefore, for both ends of this particular lattice we distinguish just four different sites, which we designate as xy, where xy = TT, TD, DT, or DD. For binding at the β-out end, x and y indicate the nucleotide contents of the β-subunits at positions p16 and p10 relative to z; for the α-out end they indicate the nucleotide contents of the β-subunits at positions m16 and m10 relative to z (see Figs. 3 and 4).

In lattice types other than the 13-A, the presence of seams means that a fixed geometry site can no longer be used. In the more general approach (see Section 2.7) the end of each protofilament is considered to be a potential site for dissociation. Likewise, the definition of an association site is relaxed to include any site in which both position p3 and position p10 are occupied, or both position m3 and position p16 are occupied (see Figs. 3 and 2).

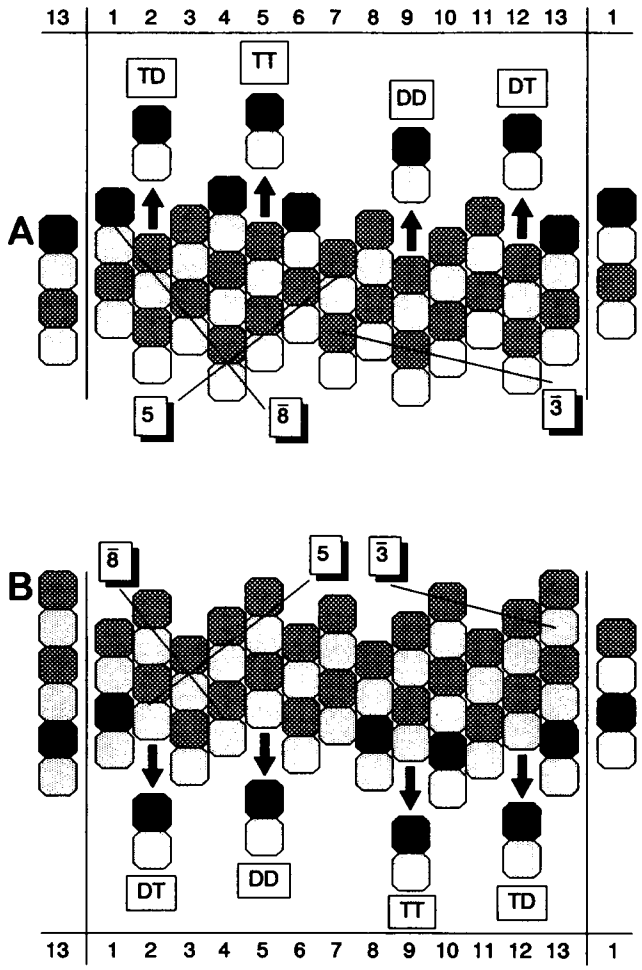

FIGURE 4 Fixed geometry binding sites at the ends of the 13- protofilament A-type microtubule lattice. (*A*) The β-out end; (*B*) the α-out end. At both ends we distinguish four sites on the basis of the nucleotide content of the β-subunit in the adjacent protofilaments using the designation xy (see text), where xy represents the 10-start related neighbor (x) and the $\overline{16}$-start related neighbor (y) relative to the binding site. Tubulin monomers are identified as α (*light shading*), β containing GTP (*black*), and β containing GDP (*cross-hatched*).

2.5. Estimation of kinetic parameters

Rate constants for association and dissociation reactions, $k_i(+)$ and $k_i(-)$ (Section 2.3, Step 2), have to be assigned for the set of sites in a self-consistent way. The free energy for the association reaction at any site, i, is related to the association constant, K_i, through the equation $\Delta G_i = -RT \cdot \ln K_i$. Thus, when the value of K_i is known one can assign values of $k_i(-)$ and $k_i(+)$ from the relationship $K_i = k_i(+)/k_i(-)$. For simplicity we generally assume that the association rate constant, $k_i(+)$, is the same for all sites; differences in affinity between sites are then reflected in the values of the dissociation rate constant $k_i(-)$.

Two approaches to the estimation of K_i values have been used:

(*a*) When a fixed-geometry binding site is used (see Section 2.4) the affinity of Tu-GTP for a particular site depends only on the nucleotide content of the tubulin molecules comprising the site, and the affinity is highest when the Tu-GTP content of the site is highest (see Section 2.1). We then assess the range of K values for the set of sites and express all other K values in terms of one assigned value (that for the TT site) plus a set of free energy difference expressions (see Section

2.6). In previous studies (13, 14, 16) we deduced that the four sites defined in Fig. 4 must have affinities for Tu-GTP that vary monotonically in the following way: TT > DT ≈ TD > DD, and this ordering generates behavior characteristic of dynamic instability. The value of K selected for the TT site is the main determinant of the calculated value of C_c and can thus be related to an experimentally determined value.

(*b*) Alternatively, the K_i values can be calculated using estimated free energy values for individual bonds. This is the only possible approach for treating the greater multiplicity of sites present when the definition of association and dissociation sites is relaxed (see Section 2.4). The affinity of a tubulin dimer for a microtubule end then depends upon the number of contacts formed, as well as on the nucleotide content of the neighboring subunits forming the binding site.

The free energy for the binding of one molecule of Tu-GTP at a particular site is seen to derive from the free energies of the specific protein-protein interactions characteristic of that site. The total free energy for binding at a particular site (ΔG_i) may be obtained as the sum of the free energies for individual subunit-subunit interactions between tubulin monomers (α, β-GTP, or β-GDP), plus a term corresponding to the free energy equivalent of the configurational entropy, ΔG_S. This configurational entropy is the free energy cost of immobilizing a dimer in the polymer (26).

2.6. Estimation of free energy differences, fixed geometry sites

We explore this simpler approach first because examination of the free energy difference values involved in the case of fixed geometry is a useful guide in the subsequent selection of individual free energy values. We base the following evaluation on the helically symmetric 13-protofilament A-lattice (Fig. 2, *A* and *B*) and consider a binding site as having the particular geometric arrangement defined previously (16) (see Section 2.4, Figs. 3 and 4).

2.6.1. Formal treatment

The binding of a molecule of Tu-GTP to a typical site (xy) (Fig. 4*A*) may be formally regarded as involving free energy terms: (*a*) ΔG_h, for the hydrolysis of the previously terminal Tu-GTP to Tu-GDP; (*b*) $\Delta G_{lattice}$, for the subsequent change in lattice contacts, and (*c*) $\Delta G_{T/xy}$, the binding reaction for site xy.

$$\Delta G_{T/xy(Total)} = \Delta G_h + \Delta G_{lattice} + \Delta G_{T/xy}$$

$\Delta G_{lattice}$ is independent of the nature of the site xy. It is generally unfavorable, since it involves lateral interactions involving Tu-GDP rather than Tu-GTP, and this is compensated by the free energy of hydrolysis. We therefore write

$$\Delta G'_{T/xy(Total)} = \Delta G_{T/xy}$$

For binding of Tu-GTP to the four different sites at the β-out end of the 13-protofilament A-lattice (Fig. 4 *A*) one may write the following free energy equations:

$$\Delta G_{T/TT} = \Delta G_{3t\alpha} + \Delta G_{10tt} + \Delta G_{3\alpha t} + \Delta G_{16tt} + \Delta G_C$$

$$\Delta G_{T/TD} = \Delta G_{3t\alpha} + \Delta G_{10tt} + \Delta G_{3\alpha d} + \Delta G_{16td} + \Delta G_C$$

$$\Delta G_{T/DT} = \Delta G_{3d\alpha} + \Delta G_{10td} + \Delta G_{3\alpha t} + \Delta G_{16tt} + \Delta G_C$$

$$\Delta G_{T/DD} = \Delta G_{3d\alpha} + \Delta G_{10td} + \Delta G_{3\alpha d} + \Delta G_{16td} + \Delta G_C$$

where the subscript T/TT indicates binding of Tu-GTP (T) to a TT site (and so on). *Note:* Specific free energy terms such as $\Delta G_{3\alpha t}$ are defined in Section 2.2. ΔG_C is equal to the sum of the free energy terms for individual interactions that are common for all sites, namely

$$\Delta G_C = \Delta G_{10\alpha\alpha} + \Delta G_{13\alpha d} + \Delta G_{16\alpha\alpha} + \Delta G_S.$$

The higher affinity of Tu-GTP for site TT, compared with site DD, for example, must derive from a difference in total free energy (i.e., $-\Delta G_{T/TT} > -\Delta G_{T/DD}$). This difference in total free energy is seen from the above equations to derive from the free energy differences for four individual lateral interactions, that is,

$$\Delta G_{T/TT} - \Delta G_{T/DD} = a + b + c + d \qquad (1)$$

where

$$a = (\Delta G_{3t\alpha} - \Delta G_{3d\alpha}),$$

$$b = (\Delta G_{3\alpha t} - \Delta G_{3\alpha d}),$$

$$c = (\Delta G_{10tt} - \Delta G_{10td}),$$

and

$$d = (\Delta G_{16tt} - \Delta G_{16td}).$$

We have previously deduced that the affinity of Tu-GTP for site TT is on the order of 100-fold greater than that for site DD. If $\{K_{T/TT}\}/\{K_{T/DD}\} = 100$, then $\Delta G_{T/TT} - \Delta G_{T/DD} = -RT \cdot \ln(100)$, and the four free energy differences (*a, b, c, d*) must sum to approximately −2.84 kcal/mol (at $T = 37°C$).

In the same way, for the sites that we have designated TD and DT one may write

$$\Delta G_{T/TT} - \Delta G_{T/TD} = b + d \qquad (2)$$

$$\Delta G_{T/TT} - \Delta G_{T/DT} = a + c \qquad (3)$$

Comparison of Eqs. 2 and 3 with Eq. 1 shows that the affinities of Tu-GTP for sites TD and DT will be intermediate between those for sites TT and DD, if all the free energy difference terms have the same sign (see below). However, the precise distribution of affinities clearly depends upon the way in which the −2.84 kcal/mol is distributed between the four difference terms.

In passing, it is readily shown using this approach that

$$\Delta G_{T/TT} + \Delta G_{lattice} = \Delta G_{D/DD}$$

and hence that $\Delta G_{T/TT(Total)} = \Delta G_h + \Delta G_{D/DD}$.

Thus, in the typical elongation step, the addition of Tu-GTP is thermodynamically equivalent to the energetically

unfavorable elongation of a Tu-GDP lattice by one molecule of Tu-GDP, which is compensated by the free energy of hydrolysis of one molecule of GTP.

For the α-out end (Fig. 4 *B*) a similar approach may be adopted. (*Note:* For convenience in the subsequent presentation the affinities of these sites are defined relative to that for the binding of Tu-GTP to the TT site at the β-out end, i.e., to $K_{T/TT}$. The corresponding equations are given in Table 1.) Furthermore, the same approach may be used to consider the free energy equations for the binding of Tu-GDP to the α- and β-out ends of the microtubule. As above, the affinities are defined relative to that for binding of Tu-GTP to a TT site at the β-out end (i.e., to $K_{T/TT}$), and the appropriate equations are again given in Table 1.

For any particular distribution of the free energy differences appearing in Table 1 one may calculate all of the appropriate ΔG and ΔG^{α} values and hence all of the K and K^{α} values for the binding of both Tu-GTP and Tu-GDP at both the α- and β-out ends. With all $k(+)_{T/xy}$ values assumed to be the same (generally $2.0 \times 10^6\ M^{-1} \cdot s^{-1}$) one can then use K and K^{α} to calculate the appropriate $k(-)_{T/xy}$ and $k(-)_{D/xy}$ values for use in the simulation. The following general principles were used in assigning values for the free-energy differences terms:

(*i*) Lateral interactions are weakened progressively when Tu-GTP is replaced by Tu-GDP; hence the four energy difference terms, which sum to −2.84 kcal (*a, b, c, d*), all have the same sign. We assume that the magnitudes of the energy difference terms are ordered as $\bar{3}$-start > 10-start > $\overline{16}$-start, and we do not generally distinguish between left- and right-handed interactions (i.e., $a = b$; $c^* = c$; $d^* = d$; see Table 1). We note that if both c^* and d^* are equal to zero then the affinity of Tu-GTP at the α-out end will not depend on the nucleotide content of the binding site (see Table 1) and dynamic behavior will not then be observed for this end.

(*ii*) The values of e and f are assumed to be greater than c and d, respectively (by extension of the assumption of the effect of substituting Tu-GDP for Tu-GTP on the strength of lateral interactions; see (*i*)).

(*iii*) The value of g ($= (\Delta G_{13\alpha d} - \Delta G_{13\alpha t})$) is important because it determines the difference in affinity between similar sites at the α- and β-out ends (see Table 1). The value of g was selected in order that the calculated affinity of Tu-GTP for sites at the α-out end should not be too high (see Table 2), and therefore that the C_c values for the two ends should be similar, in accord with experimental observations (5) (see Section 3.2). This implies that longitudinal interactions are strengthened when Tu-GTP is replaced by Tu-GDP; this is consistent with experimental evidence showing that Tu-GDP self-associates into ringlike oligomeric species more strongly than Tu-GTP (29) and that these oligomers probably represent curved protofilaments, implying strengthened longitudinal interactions of Tu-GDP (30).

2.6.2. Calculation of association constants

An example of a calculation of association constants using one particular set of free energy differences is shown in Table 2. The following points may be noted:

(*i*) Relatively small differences for the free energies of α, β-GTP, and β-GDP subunits (less than 1 kcal/mol) are sufficient to generate significant differences in affinities for the different sites. The affinities for binding of Tu-GTP to sites at the β-out end are in the order $K_{T/TT} > K_{T/TD} \approx K_{T/DT} > K_{T/DD}$, as stipulated. Dissociation rate constants for Tu-GTP are then in the order $k(-)_{T/DD} > k(-)_{T/DT} \approx k(-)_{T/TD} > k(-)_{T/TT}$.

(*ii*) The affinities for the binding of Tu-GTP to sites at the α-out end are seen to be ordered in a way similar to those for

TABLE 1 Free energy difference equations for Tu-GTP and Tu-GDP binding at four different sites at the α- and β-out ends of the 13-protofilament A-lattice (see Fig. 4, *A* and *B*)

Binding of Tu-GTP			
β-out end		α-out end	
$\Delta G_{T/TT} - \Delta G_{T/TT}$	0	$\Delta G_{T/TT} - \Delta G^{\alpha}_{T/TT}$	g
$\Delta G_{T/TT} - \Delta G_{T/DD}$	$a + b + c + d$	$\Delta G_{T/TT} - \Delta G^{\alpha}_{T/DD}$	$g + c^* + d^*$
$\Delta G_{T/TT} - \Delta G_{T/TD}$	$b + d$	$\Delta G_{T/TT} - \Delta G^{\alpha}_{T/TD}$	$g + d^*$
$\Delta G_{T/TT} - \Delta G_{T/DT}$	$a + c$	$\Delta G_{T/TT} - \Delta G^{\alpha}_{T/DT}$	$g + c^*$
Binding of Tu-GDP			
β-out end		α-out end	
$\Delta G_{T/TT} - \Delta G_{D/TT}$	$c^* + d^*$	$\Delta G_{T/TT} - \Delta G^{\alpha}_{D/TT}$	$a + b + c + d$
$\Delta G_{T/TT} - \Delta G_{D/DD}$	$a + b + e + f$	$\Delta G_{T/TT} - \Delta G^{\alpha}_{D/DD}$	$a + b + e + f$
$\Delta G_{T/TT} - \Delta G_{D/TD}$	$b + c^* + f$	$\Delta G_{T/TT} - \Delta G^{\alpha}_{D/TD}$	$a + b + c + f$
$\Delta G_{T/TT} - \Delta G_{D/DT}$	$a + d^* + e$	$\Delta G_{T/TT} - \Delta G^{\alpha}_{D/DT}$	$a + b + d + e$

$a = (\Delta G_{3t\alpha} - \Delta G_{3d\alpha})$; $b = (\Delta G_{3\alpha t} - \Delta G_{3\alpha d})$; $c = (\Delta G_{10tt} - \Delta G_{10td})$;
$d = (\Delta G_{16tt} - \Delta G_{16td})$; $c^* = (\Delta G_{10tt} - \Delta G_{10dt})$; $d^* = (\Delta G_{16tt} - \Delta G_{16dt})$;
$e = (\Delta G_{10tt} - \Delta G_{10dd})$; $f = (\Delta G_{16tt} - \Delta G_{16dd})$; $g = (\Delta G_{13\alpha d} - \Delta G_{13\alpha t})$.

TABLE 2 Association constants for Tu-GTP and Tu-GDP binding at four different sites at the α- and β-out ends of the 13-filament A-lattice (see Fig. 4, *A* and *B*)

Site (*xy*)	β-out end		α-out end	
	$10^{-4}\cdot K_{T/xy}$ (M^{-1})	$10^{-4}\cdot K_{D/xy}$ (M^{-1})	$10^{-4}\cdot K^{\alpha}_{T/xy}$ (M^{-1})	$10^{-4}\cdot K^{\alpha}_{D/xy}$ (M^{-1})
TT	100.00	18.60	19.70	1.00
DD	1.00	0.55	3.65	0.55
TD	11.40	3.90	9.70	0.90
DT	8.80	2.65	7.45	0.60

The free energy differences used in these calculations are:
a (= $\Delta G_{3t\alpha} - \Delta G_{3d\alpha}$) = b(= $\Delta G_{3\alpha t} - \Delta G_{3\alpha d}$) = −0.9 kcal;
c (= $\Delta G_{10tt} - \Delta G_{10td}$) = c^*(= $\Delta G_{10tt} - \Delta G_{10dt}$) = −0.6 kcal;
d (= $\Delta G_{16tt} - \Delta G_{16td}$) = d^*(= $\Delta G_{16tt} - \Delta G_{16dt}$) = −0.44 kcal;
e (= $\Delta G_{10tt} - \Delta G_{10dd}$) = −0.9 kcal;
f (= $\Delta G_{16tt} - \Delta G_{16dd}$) = −0.5 kcal;
g (= $\Delta G_{13\alpha d} - \Delta G_{13\alpha t}$) = −1.0 kcal.

binding at the β-out end, but they span a much narrower range. This is because the bonds in the $\bar{3}$-start direction (3αt and 3tα) are common for all binding sites at the α-out end (see Fig. 4 *B*) and hence difference terms involving these bonds do not appear (see Table 1). Thus, the differences between the various sites at the α-out end depend only upon differences for interactions in the 10- and $\overline{16}$- start directions, that is, energy difference terms c^* and d^* (see above).

(*iii*) The affinity of Tu-GDP for the DD site at the β-out end is predicted to be very low (see Table 2), so that assembly of pure Tu-GDP will occur only at very high total protein concentration. Consideration of the equations in Table 1 shows that Tu-GDP should, however, have a significantly higher affinity for GTP-containing sites (especially the TT site) at the β-out end. The implications of these properties are discussed below.

(*iv*) Relatively low affinity binding of Tu-GDP is predicted for all sites at the α-out end, irrespective of their nucleotide content.

2.7. The general treatment

As noted above, consideration of the additional lattices (13-B, 14-A) introduces a greater complexity of the subunit-subunit interactions and requires a more generalized approach, involving estimation of individual free energy values. In assigning values of free energies for specific interactions, we use the free energy differences discussed in Section 2.6 as a guide and apply the following general principles, which will then be equally applicable to all types of lattice:

(*i*) Since two intrinsically different lattice interactions are known to exist (i.e., both A and B), involving either heterologous (A: α-β) or homologous (B: α-α, β-β) interactions along the $\bar{3}$-start helix, we conclude that the sum of all of the free energies for interactions of a Tu-GDP dimer with neighboring dimers in the A-lattice is likely to be rather similar to that for a Tu-GDP in the B-lattice. In other words, we are assuming that seams are not necessarily a source of either stability or instability, and free energy terms are selected accordingly.

(*ii*) For interactions between any particular two subunit types, those in the $\bar{3}$-start direction are generally assumed to be stronger than those in the 10-start direction, and these, in turn, are generally stronger than those in the $\overline{16}$-start direction (e.g., $-\Delta G_{3tt} > -\Delta G_{10tt} > -\Delta G_{16tt}$; cf. Section 2.6.1(*i*)).

(*iii*) For each of the lateral lattice directions ($\bar{3}$, 10, and $\overline{16}$), the interactions involving GTP-containing β-subunits are assumed to be stronger than those involving GDP-containing β-subunits (thus, e.g., $-\Delta G_{3t\alpha} > -\Delta G_{3d\alpha}$). In contrast, for the longitudinal bond the opposite is the case, and we generally consider that $-\Delta G_{13da} > -\Delta G_{13ta}$ (see Section 2.6.1(*iii*)).

(*iv*) The value for ΔG_S has been estimated by Erickson (26) to lie in the range 7 to 11 kcal/mol. We arbitrarily assign ΔG_S to be 9 kcal/mol, the midpoint of this range.

The set of free energy values used in all simulations reported here is given in Table 3. This table also shows calculated values of association constants for the four fixed-geometry binding sites of the 13-A lattice previously considered in the simple treatment (cf. Table 2). These new calculations again give association constants for the binding of Tu-GTP at the β-out end in the order $K_{T/TT} > K_{T/TD} \approx K_{T/DT} > K_{T/DD} > K_{D/DD}$ (see Table 3). The binding constants for Tu-GTP at the α-out end are ordered in a similar way and again cover a much narrower range of affinities, as in the case of the simpler treatment. The predictions for the binding of Tu-GDP are also similar to those

TABLE 3 Association constants for Tu-GTP and Tu-GDP binding at four different sites at the α- and β-out ends of the 13-filament A-lattice (see Fig. 4, *A* and *B*) calculated using individual free energy terms

Site (*xy*)	β-out end		α-out end	
	$10^{-4}\cdot K_{T/xy}$ (M^{-1})	$10^{-4}\cdot K_{D/xy}$ (M^{-1})	$10^{-4}\cdot K^{\alpha}_{T/xy}$ (M^{-1})	$10^{-4}\cdot K^{\alpha}_{D/xy}$ (M^{-1})
TT	499.00	98.40	31.60	2.00
DD	2.00	0.55	6.20	0.55
TD	37.20	7.30	16.5	1.05
DT	26.80	7.30	11.92	1.05

The individual free energy values used in these calculations are (see text):
ΔG_S = 9 kcal/mol;
$\Delta G_{13\alpha d}$ = −9.9; $\Delta G_{13d\alpha}$ = −9.9; $\Delta G_{13t\alpha}$ = −8.2; $\Delta G_{13\alpha t}$ = −8.2;
ΔG_{3tt} = −3.0; ΔG_{3dt} = −1.7; ΔG_{3td} = −1.7; ΔG_{3at} = −2.1;
$\Delta G_{3ta\alpha}$ = −2.1; ΔG_{3dd} = −0.6; $\Delta G_{3\alpha\alpha}$ = −0.6; $\Delta G_{3\alpha d}$ = −0.9; $\Delta G_{d\alpha}$ = −0.9;
ΔG_{10tt} = −1.8; ΔG_{10dt} = −1.2; ΔG_{10td} = −1.2; $\Delta G_{10\alpha t}$ = −1.4; $\Delta G_{10t\alpha}$ = −1.4;
ΔG_{10dd} = −0.8; $\Delta G_{10\alpha\alpha}$ = −0.8; $\Delta G_{10\alpha d}$ = −0.9; $\Delta G_{10d\alpha}$ = −0.9;
ΔG_{16tt} = −1.3; ΔG_{16dt} = −0.9; ΔG_{16td} = −0.9; $\Delta G_{16\alpha t}$ = −1.1; $\Delta G_{16t\alpha}$ = −1.1;
ΔG_{16dd} = −0.5; $\Delta G_{16\alpha\alpha}$ = −0.5; $\Delta G_{16\alpha d}$ = −0.6; $\Delta G_{16d\alpha}$ = −0.6.
The corresponding free energy differences (see Table 2) are:
$a = b$ = −1.2 kcal/mol; $c = c^*$ = −0.6 kcal/mol;
$d = d^*$ = −0.4 kcal/mol; e = −1.0 kcal/mol;
f = −0.5 kcal/mol; g = −1.7 kcal/mol.

made by the simple treatment. The affinity is calculated to be rather high for binding of Tu-GDP at the TT site at the β-out end but low for all Tu-GDP binding at all other sites at the α- and β-out ends.

The choice of a relatively high free energy (and thus strength) for the longitudinal bond is consistent with the view that longitudinal bonds are stronger than lateral ones (31, 32). In terms of the previous discussion the addition of a subunit to the standard geometry site of the 13-A lattice creates six lateral bonds and one longitudinal bond (see Section 2.6.1). Inspection of Fig. 2 shows that, for the 13-B and 14-A lattices, some association events at sites adjacent to the "seam" (e.g., those at the ends of protofilaments 8 and 9 in the 14-A lattice shown in Fig. 2 *D* and that at the end of protofilament number 9 in the 13-B lattice shown in Fig. 2 *C*) result in the formation of only four lateral bonds. Therefore, if the lateral bonds make too large a relative contribution to the overall free energy of binding, these particular sites will be of very low affinity and will be kinetically disfavored during periods of growth. Furthermore, dimers bound at sites with more than six lateral bonds (such as, e.g., those created following the addition of subunits to both protofilaments 8 and 9 of the 14-A lattice in Fig. 2 *D*) would be bound with very high affinity and would impair dissociation.

3. RESULTS

With this new formulation, the kinetic properties can be evaluated for any of the lattices described here and indeed for any other lattice of mixed A, B type. The general treatment (Section 2.7) relaxes the previous requirement to define sites in terms of a specific structure for association/dissociation and allows a free energy value (and hence an association constant) to be assigned for binding at sites with any number and type of neighbors. Thus, the general treatment uses the same free energy assignments for particular subunit-subunit interactions with specified spatial relationship ($\bar{3}$, 10, 13, $\bar{16}$) and nucleotide composition (α, β-ATP, β-ADP) irrespective of the overall lattice type and symmetry. Some of the results obtained from applying this new treatment to the β-out ends of the 13-A, 13-B, and 14-A microtubule lattices and to the α-out end of the 13-A microtubule lattice will now be discussed. These data derive from extended length versus time plots as described in Section 2.3.

3.1. Growth-shortening transitions

Fig. 5 *a* shows that simulation of the 13-A microtubule lattice under conditions of zero net growth (i.e., [Tu-GTP] = C_c) produces the growth-shortening behavior characteristic of dynamic instability. This result is consistent with results previously reported for the "fixed geometry" formulation of the problem (14). The microtubule behavior is well characterized in terms of a single growth rate and a single shortening rate, although closer inspection shows some variation in rate

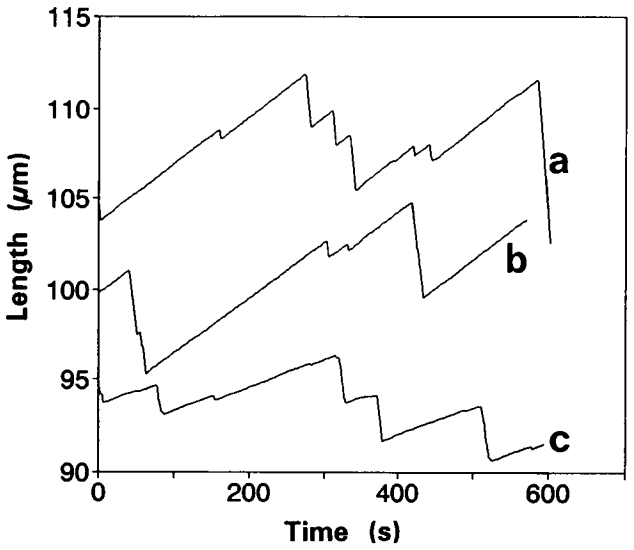

FIGURE 5 Simulated length changes as a function of time for three different microtubule lattices. Plots for the 13-A (*a*), 14-A (*b*), and 13-B (*c*) lattices, simulated using the general method for deriving rate constants for different lattice configurations, as described in the text. The simulations were performed at the appropriate C_c for each lattice (see Fig. 6).

(see Section 3.5). The $L(t)$ plot (Fig. 5, *plot a*) shows that transitions (G→S and S→G) occur frequently but apparently randomly; the amplitude (or duration) of either phase likewise shows an apparently random distribution. Some of the smaller length excursions might easily be below the resolution of direct observations.

Fig. 5 (*plots b* and *c*) shows that the phenomenon of transitions is not restricted to the 13-A lattice; the inclusion of a single B-type seam in the 14-A lattice has almost no effect. With the exception of protein-protein contacts at the seam itself, the lattice is effectively identical to the 13-A lattice, and the dynamic properties are similar. For the 13-B lattice, as seen in Fig. 2 *C*, the geometry involves essentially a single A-type seam in a B-type lattice. Nonetheless, at the C_c, dynamic transitions are clearly evident, although intrinsic rates of growth and shortening phases, and length excursions, are generally smaller. These effects are mainly due to the different end configurations of the B-type lattice (see below). Thus, dynamic instability is not solely the property of the helically symmetric 13-A lattice. All lattices typically show transitions between growth and shortening, but with characteristic differences.

3.2. Net growth properties

The plots of net growth rate versus [Tu-GTP] (or $J_{on}C$ plots) have a similar form for the β-out ends of all three lattices, with similar values for the C_c in the range 8–10 μM, as shown in Fig. 6. While the 14-A lattice shows properties similar to those of the 13-A lattice, it is notable that the 13-B lattice has a slower bimolecular rate constant for microtubule growth (the limiting slope at high [Tu-GTP]) and a lower maximum shortening rate (at [Tu-GTP] = 0). This is because there are

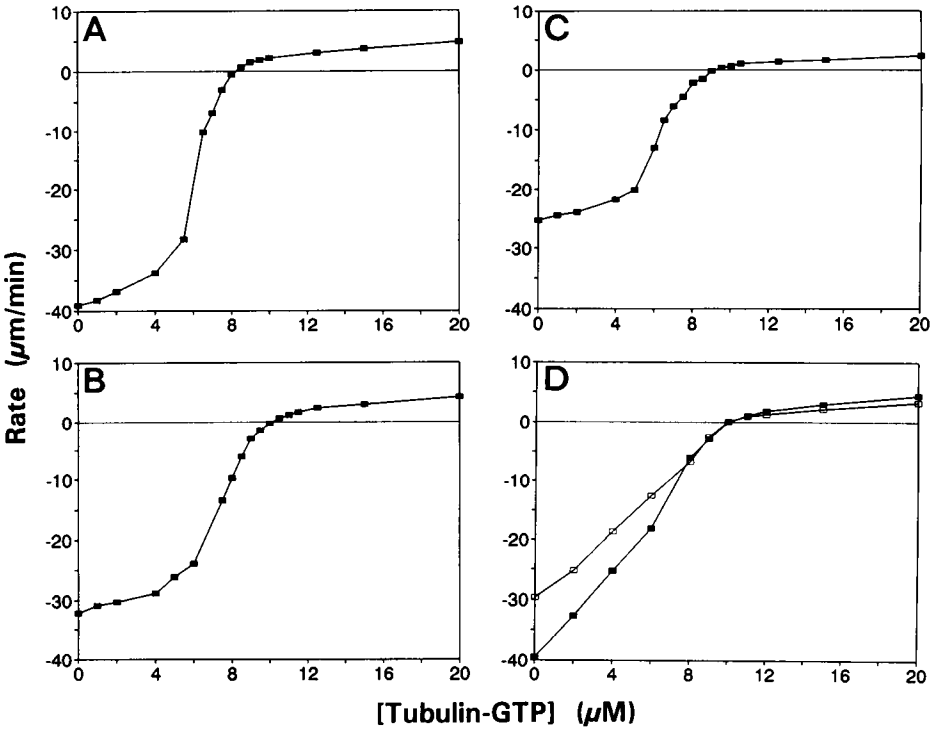

FIGURE 6 Macroscopic microtubule population growth properties for three different microtubule lattices. $J_{on}c$ plots for the β-out ends of the 13-A (*A*), 14-A (*B*), and 13-B (*C*) lattices and for the α-out end of the 13-A lattice (*D*). (*D*) also shows the effect of changing $k(+)_{T/xy}$ from 2.0×10^6 (*filled symbols*) to 1.50×10^6 $M^{-1}\cdot s^{-1}$ (*open symbols*). The curves show net growth rate as a function of [Tu-GTP]. Each point derives from an extended simulation of *L(t)* as in Fig. 5, to assess the net growth (or shortening) as a function of time at a given Tu-GTP concentration.

fewer energetically favorable sites for association (and dissociation) on the 13-B lattice (an average of 1.63) than on the 13-A lattice (an average of 3.33). Nonetheless, dynamic transitions between growth and shortening are predicted (as shown in Fig. 5).

The $J_{on}C$ plot for the α-out end of the 13-A lattice (Fig. 6 *D*) is predicted to have a shape different from that for the β-out end, as reported previously (16). As the concentration of Tu-GTP is lowered below the C_c, the rate of shortening increases steadily and approaches the maximum value at [Tu-GTP] = 0. This difference between the observed and maximum shortening rates is due to two factors. At very low Tu-GTP concentrations, it is due solely to isolated Tu-GTP addition events, almost entirely at DD sites, whereas at concentrations closer to the C_c, there are short periods of growth that produce a very much lower net shortening rate. The isolated addition events are more effective in reducing the shortening rate for the α-out end. This is because (see Table 3) the affinity of Tu-GTP for a DD site is predicted to be higher at the α-out end compared with the β-out end. One other feature deserves comment. The maximum shortening rate (at [Tu-GTP] = 0) is seen to be the same for both the α- and β-out ends (Fig. 6, *A* and *D*). This is because the affinity of Tu-GDP for DD sites with the same geometry has to be the same for both ends (see Table 3), and since the same association rate constant has been assumed for all sites (see Section 2.5), the dissociation rate is necessarily the same.

In fact, considerable experimental evidence exists that the experimentally observed association rate constant for the addition of Tu-GTP is different at the opposite ends of the microtubule (5, 33). Recent work has confirmed this fact, with direct observations of individual microtubules under a range of conditions of protein concentration and temperature (K. K. Sharma, S. R. Martin, and P. M. Bayley; manuscript in preparation). The higher value is the "plus end," which is generally presumed to be the β-out end. It is therefore probably more realistic to assign a lower value of $k(+)_{T/xy}$ to the α-out end. Since the dissociation rate constants $(k(-)_{T/xy}$ and $k(-)_{D/xy}$ are reduced by a similar factor (considerations of the affinities being unchanged), this also leads to a lower value of the maximum shortening rate (determined by the value of $k(-)_{D/DD}$) at the α-out end (see Fig. 5 *D*), while the C_c remains unchanged. However, as indicated in Section 2.61, differences in critical concentration at the two ends are determined by the value assigned to the free energy difference *g* (Tables 1–3) deriving from the value of $\Delta G_{13\alpha t}$ relative to $\Delta G_{13\alpha d}$. With the values given in Table 3, the C_c for the α-out end is 10.1 μM, compared with 8.25 μM for the β-out end. It is found that the critical concentration for the α-out end would decrease from 10.1 to 6.2 μM as $\Delta G_{13\alpha t}$ changes from −8.2 to −8.7 kcal/mol and *g* changes from −1.7 to −1.2 kcal/mol. This illustrative calculation therefore shows that a difference of free energy of interaction as small as 0.5 kcal for the longitudinal intermolecular interaction of the α-subunit with β-GTP compared with β-GDP could have a marked effect on the relative critical concentrations of the two ends. Such an energy difference is entirely plausible, since it is small compared to hydrogen bond formation, charge interactions, or an additional bivalent ion interaction. This demonstrates that differences in affinity and kinetics at opposite ends may be due to extremely small differences in specific, end-dependent, subunit-subunit interactions.

3.3. Transition behavior

Fig. 7 (*A* and *B*) shows the variation in mean growth and shortening rates for all three microtubule lattices in the range of [Tu-GTP] spanning the C_c for each. The growth rate remains linearly dependent upon [Tu-GTP] in this range, whereas the shortening rate is in each case considerably less than the rate at [Tu-GTP] = 0, due to the presence of mixed-end intermediates such as structures D and E of Fig. 1.

For all three lattice types, the mean lifetimes of both growth (T_g) and shortening (T_s) are predicted to have a marked nonlinear dependence on [Tu-GTP] for both ends of the microtubule (Fig. 7, *C* and *D*; see also Ref. 14). This condition, which is necessary for the related phenomenon of oscillatory microtubule growth (7, 34), tends to restrict dynamic instability to a relatively narrow range of [Tu-GTP] about the C_c. Early experimental observations (5) showed an apparently linear dependence of transition rates ($1/T_g$ and $1/T_s$) on [Tu-GTP]. However, contrary to the view given by Caplow (11), more recent measurements (35) have confirmed that the rates are indeed nonlinearly dependent on [Tu-GTP], as required for the two-state transition behavior (7, 14). Fig. 8 plots this experimental data (logarithmically, as in Ref. 35) with the calculations for the transition frequencies for both ends of the 13-A lattice (the plus and minus ends are defined operationally as having higher and lower growth rates; these correlate with the calculated properties for the β- and α-out ends). For both G→S and S→G transitions the approximate relationship between log(frequency) and [Tu-GTP] is shown by both experimental and simulated data. For the S→G transition, there is a systematic difference, with calculated frequencies for the 13-A lattice generally higher than the available experimental results. No attempt has been made to adjust the model parameters in order to fit the experimental data. As shown elsewhere (15) the number of observations of transitions (and hence lifetimes) required to provide a reliable average for the frequencies is difficult to achieve experimentally, particularly for concentrations much above or below the C_c. The important prediction of the model, namely the nonlinear dependence on [Tu-GTP], is well substantiated for the G→S regime.

Walker et al. (35) also demonstrated that growing microtubules diluted to very low [Tu-GTP] experienced a growth to shortening transition ("catastrophe") within 4–6 s of dilution and that this time interval was independent of the rate of growth of the microtubule (observed at different [Tu-GTP] values) prior to the dilution. This observation was very important, because it showed that the size of any capping structure must be independent of the rate of growth. This is consistent with the postulate of coupling between Tu-GTP addition and GTP hydrolysis, which is central to the formulation of the lateral cap model (see Section 2.1). Simulations for the β-out end of the 13-A lattice show that growing microtubules diluted to 0, 1, and 2 μM Tu-GTP undergo a growth-to-shortening transition after (on average) 2.8 (±0.7), 4 (±1.3), and 6.7 (±2.1) s, respectively, and that this time is independent of the initial [Tu-GTP] present in the starting (predilution) conditions. These results are fully consistent the observations of Walker et al. (35).

Microtubule growth off seeds at [Tu-GTP] < C_c shows interesting biochemical features (36). Under dynamic conditions, short microtubules nucleate and extend to lengths that can be detected by electron microscopy (Ref. 37 and M. F. Symmons, S. R. Martin, and P. M. Bayley, unpublished observations). Simulations with the model show that these microtubules have a high probability of undergoing the G→S transition and hence frequently shorten back to zero length. The rate of GTP hydrolysis increases approximately linearly with [Tu-GTP], corresponding to the bimolecular addition reaction, once the terminal tubulin-GTP layer is established. The nonlinear relationship (rate proportional to [Tu-GTP]^2),

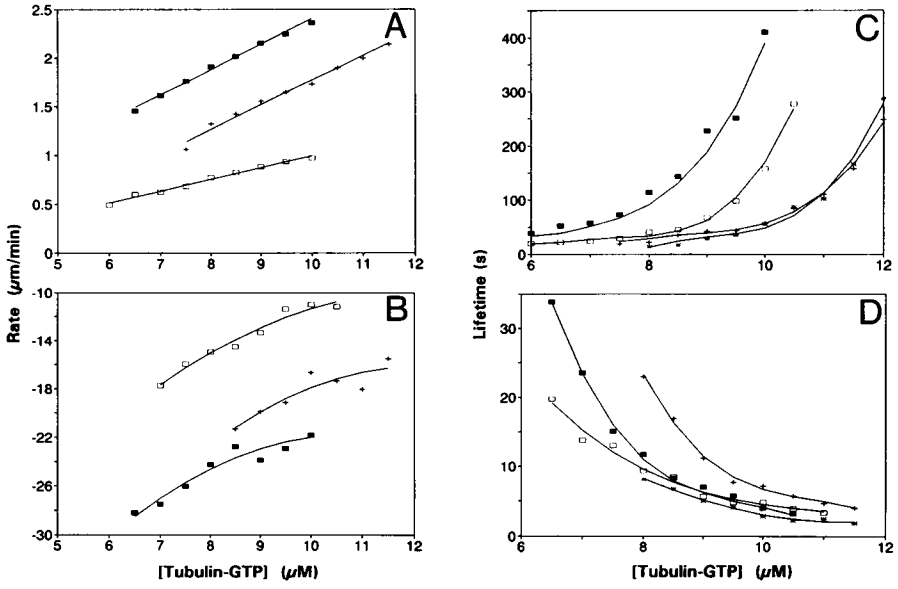

FIGURE 7 Mean state lifetimes, growth rates, and shortening rates as a function of [Tu-GTP] for three different microtubule lattices. (*A*) Growing rates (R_g) as a function of [Tu-GTP] for the β-out ends of the 13-A (■), 13-B (□), and 14-A (+) lattices. (*B*) Shortening rates (R_s) as a function of [Tu-GTP] for the β-out ends of the 13-A (■), 13-B (□), and 14-A (+) lattices. (*C*) Growing state lifetime (T_g) as a function of [Tu-GTP] for the β-out ends of the 13-A (■), 13-B (□), and 14-A (+) lattices and for the α-out end of the 13-A lattice (*). (*D*) Shortening state lifetime (T_s) as a function of [Tu-GTP] for the β-out ends of the 13-A (■), 13-B (□), and 14-A (+) lattices and for the α-out end of the 13-A lattice (*).

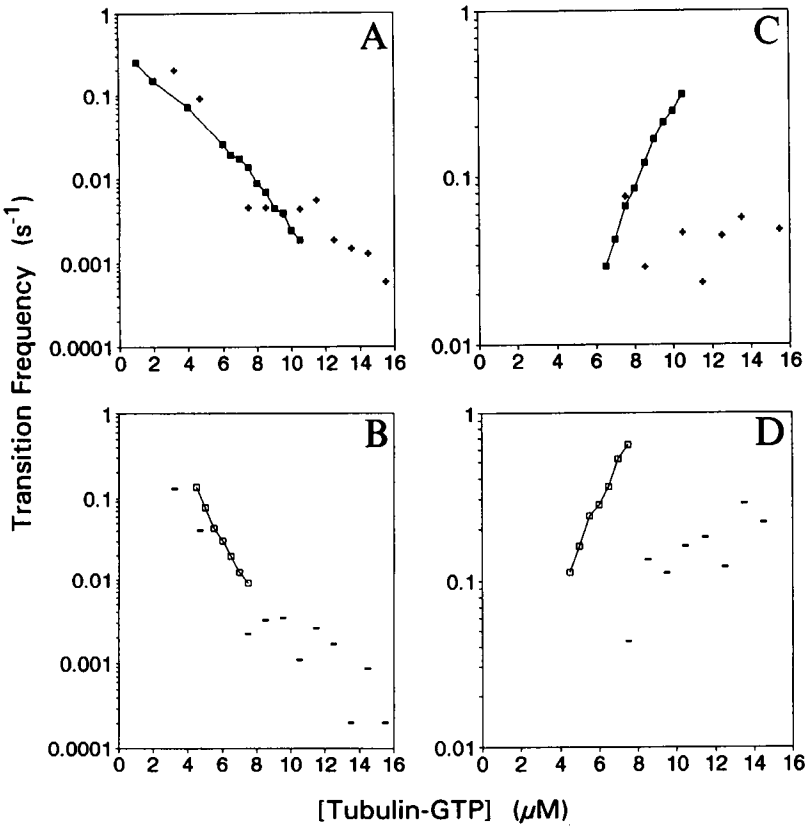

FIGURE 8 Frequencies of G→S (*A* and *B*) and S→G (*C* and *D*) transitions as a function of [tubulin-GTP]. Comparison of computed values for the β-out (■) and α-out (□) ends of the 13-protofilament A-lattice with experimental values taken from Walker et al. (5, 35) (+, plus end; –, minus end). *Note:* Frequencies are the reciprocals of the mean state lifetimes, T_s and T_g.

suggested by Caplow (11), does not appear to be significant once finite growth occurs.

We note that the lifetime for the shortening state at the α-out end is predicted to be rather short. This is because (see Table 3 and above) the addition of Tu-GTP to a DD site at the α-out end (the initial step in any rescue process at this end) is predicted to occur with relatively high affinity.

3.4. The nature of the microtubule ends

While the free-energy relationships derived in this treatment ensure that there are a relatively small number of energetically preferred steps, none of the possible dissociation events are excluded a priori, and hence energetically unfavorable steps, such as the dissociation of a dimer from a partially buried lattice position, may occur. The infrequent occurrence of such events does have important consequences for the predicted behavior of the microtubule end during the simulation.

Ultrastructural observations (using negative staining) suggest that assembling microtubules may exhibit "frayed" ends, but disassembling ends may be smoother (38). However, in frozen hydrated preparations, assembling microtubules appear to be more regular, but rapidly disassembling ones show protofilament fraying (31). Simulations with the fixed geometry binding site (see above) must, of course, necessarily produce smooth-ended microtubules in both the growth and shortening phases. However, because the new simulation procedure employed here allows energetically unfavorable events to occur with low probability, the microtubule end is quite often seen to be irregular, with one or more long extensions consisting of a few protofilaments. This extension exists when the extended protofilaments are the only ones capped by Tu-GTP; these are then stabilized (by lateral interactions between the terminal Tu-GTPs) while the other, uncapped protofilaments rapidly dissociate from around the stabilized region. In this connection it is important that the free energy for binding is partitioned predominantly in favor of the longitudinal interactions.

Calculations show that for the 13-A lattice, approximately 82% of all dissociation events and more than 99% of all association events occur at the set of sites (see Figs. 3 and 4) that we have used in our previous simulations using the fixed geometry approach. Thus, as formulated, the simulations suggest that protofilament extensions would be much more common during rapid shortening, especially during the transition from growth to shortening behavior. It may be noted that conditions that promote rapid disassembly (e.g., elevated concentrations of divalent cations) (39, 40) also promote the formation of oligomeric species (29). The rate enhancement may be due to a change in the mechanism of dissociation involving either oligomeric species as the dissociating form or the induction of gross structural effects. Neither of these possibilities is considered in these simulations.

3.5. Variability in growth and shortening rates

Data have been presented recently suggesting that microtubules may grow at intrinsically different rates in vitro (41). These authors have reported that growth (and shortening) of individual microtubules in seeded assembly of tubulin dimer show variations in rate over short time scales during a single period of growth (or shortening). The $L(t)$ plots reported here (Fig. 5) show only rather limited microscopic variations in rate within a given phase. This is due to the variation in the number of sites for association and dissociation and to the existence of "imperfect" or "mixed" ends with exposed terminal Tu-GDP molecules (10). However, these factors are probably not able to explain major variations in rate. A more probable source of more persistent variations could be a change of lattice type (A or B) within a single microtubule, which would simultaneously introduce a new set of contacts. Also, there is the possibility of a change of protofilament number within a single microtubule. These have been observed but only with low frequency, for example, approximately every 15 μm (21). This would constitute a potentially mobile defect, so the point at which a change of rate might occur need not be stationary. Fig. 7 *A* shows that the growth rates of 13-A and 14-A lattices differ by a factor of approximately 1.5 at 8 μM Tu-GTP; the more major structural change in the 13-B type lattice has a greater effect, and mixed A/B lattices may be expected to show intermediate behavior. Alternatively, at the microscopic level, microtubule elongation may be a more irregular process than simple helical growth. The fact that antiparallel protofilament orientations are observed (in sheet structures) suggests that the occasional addition of an individual tubulin dimer in an antiparallel orientation might be energetically possible, and this could produce additional kinetic complexity.

3.6. The effect of small ligands on microtubule dynamic instability

Effects of GDP

The simulations described so far have considered only the case where free tubulin is present as Tu-GTP. Experimentally, this is usually achieved by including an enzymic system for the rapid regeneration of Tu-GTP from the Tu-GDP liberated by microtubule shortening. It is clearly of interest to consider explicitly the effects on microtubule dynamics of including Tu-GDP as a component of the system. Inspection of the predicted association constants for binding of Tu-GDP to a GDP-containing site (Table 3) shows that assembly of Tu-GDP is not expected to occur under normal buffer conditions. This is in agreement with the experimental observations that microtubule assembly from pure Tu-GDP is effectively excluded. However, the relatively high affinity of Tu-GDP for a GTP-containing site at the β-out end suggests that the binding of Tu-GDP could have a significant effect on microtubule behavior when present with Tu-GTP. Simulations using mixtures of Tu-GDP and Tu-GTP show that adding GDP would, on our model, increase the observed critical concentration (as expected) and suppress dynamics, even at relatively low levels. Thus, for example, Fig. 9 shows that the presence of as little as 10% Tu-GDP increases the C_c from 8.25 to 12.5 μM (Fig. 9 *A*) and dramatically reduces the size of the length excursions (Fig. 9 *B*). This suggests that the presence of a relatively small molar fraction of tubulin as Tu-GDP may have surprisingly large effects on observable dynamic properties. More specifically, in situations where Tu-GDP is likely to accumulate even transiently (as in oscillatory systems studied at relatively high protein concentrations), direct effects of Tu-GDP will need to be considered explicitly.

Effects of nonhydrolyzable analogues

The behavior of a nonhydrolyzable analogue (such as GMP-PNP) is readily simulated by "switching off" the hydrolysis

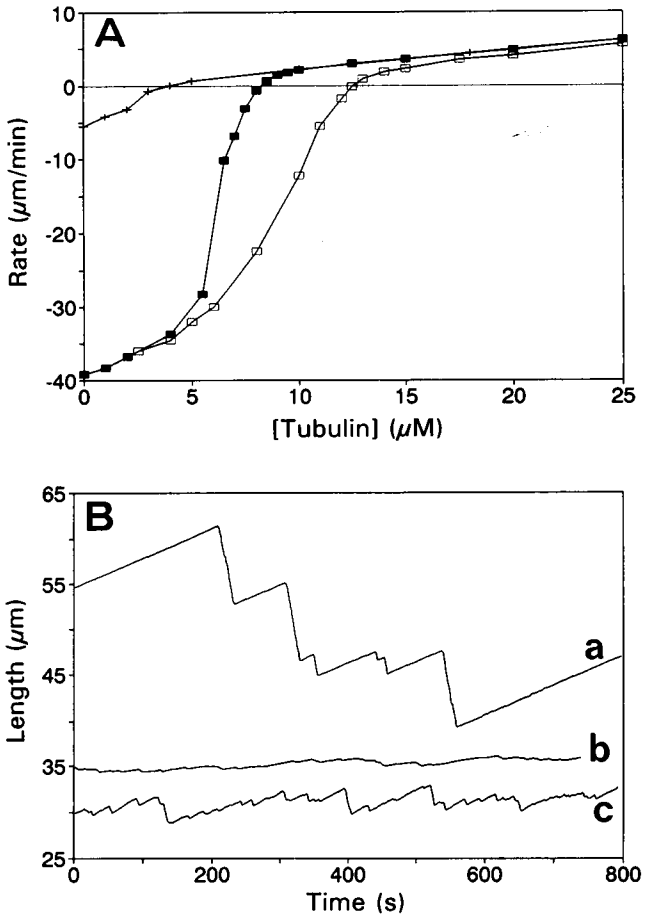

FIGURE 9 Effects of GDP and a nonhydrolyzable GTP analog (e.g., GMPPNP) on microtubule dynamics. (*A*) $J_{on}c$ plots for the β-out end of the 13-A lattice for Tu-GTP alone (■), for Tu-GTP containing 20% Tu-GMPPNP (+), and for Tu-GTP containing 10% Tu-GDP (□). (*B*) Length versus time plots for the β-out end of the 13-A lattice for Tu-GTP alone (*a*), for Tu-GTP containing 20% Tu-GMPPNP (*b*), and for Tu-GTP containing 10% Tu-GDP (*c*). The simulations were performed at the appropriate C_c for each mixture (see *A*).

step. In the simplest treatment we assume that tubulin containing a nonhydrolyzable analogue behaves in the same way as Tu-GTP. The affinity of a tubulin molecule for the microtubule end does not then depend on nucleotide content for pure Tu-GMPPNP, and one obtains a linear $J_{on}C$ plot with a low critical concentration (~1 μM for the β-out of the 13-protofilament A-lattice, compared with 8.25 μM for Tu-GTP). This is consistent with experimental observations (42). Simulations on mixtures of Tu-GTP and Tu-GMPPNP (for example) show that relatively small amounts of Tu-GMPPNP in the mixture reduce the C_c (e.g., from 8.25 to 3.9 μM at 20% Tu-GMPPNP; Fig. 9 *A*) and suppress dynamics by reducing growing and shortening state lifetimes (Fig. 9 *B*). Furthermore, incorporation of relatively small amounts of Tu-GMPPNP in the lattice produces a microtubule that disassembles rather slowly; the maximum disassembly rate is reduced by more than a factor of 6 when only 20% Tu-GMPPNP is incorporated (Fig. 9 *A*).

Suitability of the microtubule lattice

The free-energy values derived for the treatment of dynamic instability given here also allow treatment of the intrinsic stability of the microtubule lattice. For example, the association constant for a Tu-GDP completely buried in the microtubule wall is calculated to be $\sim 1.5 \times 10^{14}$ M^{-1}. Assuming an association rate constant of 2.0×10^6 $M^{-1} \cdot s^{-1}$, the calculated dissociation rate constant for this dimer is $\sim 1.3 \times 10^{-8}$ s^{-1} (43). This value is in remarkable agreement with that derived by Dye et al. (32) from the experimental observation of the breakdown rate of microtubules "tethered" at both ends. While this is no more than an order of magnitude calculation, it does emphasize the kinetic barrier to loss of Tu-GDP from the microtubule wall, due to the lattice interactions. Thus, endwise depolymerization is the strongly preferred physical mechanism in which the most important step is the loss of individual molecules of Tu-GDP from sites containing only Tu-GDP.

Substoichiometric inhibition of microtubule dynamics by antimitotic drugs

We have previously shown experimentally (44) that the primary action in vitro of the antimitotic drug podophyllotoxin is to suppress the dynamic transitions of microtubules. Similar data have been obtained for colchicine (A. Vandecandelaere, M. J. Schilstra, S. R. Martin, and P. M. Bayley, manuscript in preparation). The lateral cap model provides an instructive basis for the simulation of such properties (15, 45). If a tubulin-drug complex (Tu-X) binds to the lattice with normal kinetics but then inhibits the addition of further molecules of Tu-GTP, the general effect is the rapid suppression of the length excursions. This is illustrated for the 13-protofilament A-type lattice in Fig. 1, where different types of inhibition are considered. In Fig. 1 *G* the presence of Tu-X (on protofilament 5) inhibits addition at the 5-start related site (protofilament 6); in Fig. 1 *H* the presence of Tu-X (on protofilament 6) inhibits addition at the $\bar{8}$-start related site (protofilament 5); in Fig. 1 *I* the presence of Tu-X inhibits both the 5- and $\bar{8}$-start related sites. Given the closed nature of the cylindrical lattice (in terms of 5- and $\bar{8}$-start related helices) the microtubule end adopts a typical configuration as shown. For example, in Fig. 1 *G*, the main activity is dissociation from protofilament 1 and its neighbors, but the end returns to the limiting configuration as shown until Tu-X either dissociates from protofilament 5 or is finally buried in the lattice by the (energetically unfavorable) addition at protofilament 6. The latter incorporation of Tu-X would be strongly substoichiometric, as reported by Skoufias and Wilson (46). Simulations show that either type 1 (Fig. 1, *G* and *H*) or type 2 interactions (Fig. 1 *I*) produce substantial inhibition of microtubule growth and thus suppression of dynamics at concentrations of Tu-X strongly substoichiometric relative to Tu-GTP (see Fig. 10). The plausibility of such a steric mechanism resides in the fact that these antimitotic drugs are of such a physical size as to interfere significantly with lateral interactions within the lattice. Suppression of dynamics has now been observed directly in individual microtubules with a number of antimitotic drugs (Refs. 47 and 48 and K. K. Sharma, A. Vandecandelaere, and P. M. Bayley, unpublished observations). The extension of these concepts leads to a general mechanism for the control of microtubule dynamics by the substoichiometric action at

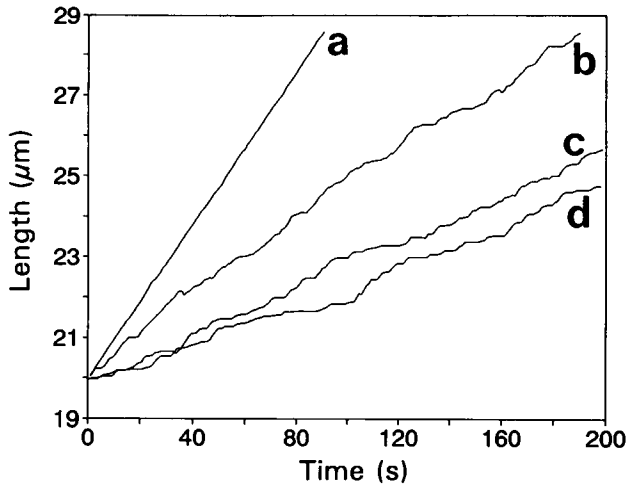

FIGURE 10 Effect of substoichiometric concentrations of drugs on microtubule growth and dynamics. Microtubule elongation at the β-out end of the 13-A lattice is simulated at a total tubulin concentration of 25 μM. (*a*) Tu-GTP alone; (*b–d*) Tu-GTP containing 1 mol % of a tubulin-drug complex. The presence of the tubulin-drug complex reduces the association rate constant for Tu-GTP into a site with a neighboring tubulin-drug molecule by a factor of 100 times. In (*b*), the tubulin-drug complex inhibits addition in both the 5 and $\bar{8}$-start related positions (Fig. 1 *I*, protofilament 4 or 6). In (*c*) it inhibits addition in the 5-start related position only (Fig. 1 *G*, protofilament 6). In (*d*), it inhibits addition in the $\bar{8}$-start related position only (Fig. 1 *H*, protofilament 5). Note the strong inhibition of growth rate and the irregularity of microtubule growth in the presence of concentrations of tubulin-drug complex highly substoichiometric to that of free Tu-GTP.

the microtubule end of potential regulatory factors, interfering with addition reactions in specific lattice directions.

4. GENERAL DISCUSSION

Previous work on the simulation of microtubule dynamic instability by Chen and Hill (17) sought to model the transition behavior of microtubules that included (in the growing state) a substantial "cap" of Tu-GTP. The more recent analytical evidence indicates that Tu-GTP in microtubules at steady state is experimentally undetectable. The lateral cap formulation was made to show how a minimal capping structure restricted in size to one Tu-GTP/protofilament end could still confer the unique dynamic properties of the microtubule system. The present work indicates the potential of this minimal model. Further elaboration (e.g., by explicitly including intermediates such as Tu-GDP-P_i or transient conformational states of bound tubulin species) is not, at present, kinetically justified.

Thus, the lateral cap model provides a relatively simple numerical treatment of the unusual dynamic properties of microtubules assembled in vitro from pure Tu-GTP. Based upon two postulates (Section 2.1) of coupled hydrolysis of Tu-GTP and the progressive destabilizing influence of the presence of Tu-GDP in the microtubule end, the characteristic two-phase growth-shortening behavior is readily reproduced. The treatment predicts that the transitions between states will be strongly influenced by [Tu-GTP], as found experimentally (see Section 3.3). The present work indicates that the original treatment of the 13-protofilament A-type microtubule lattice is readily extended to treat microtubule lattices of different symmetry types. The important conclusion is that, on this model, dynamic instability is not the exclusive property of the helically symmetric 13-protofilament A-type lattice of the tubulin α-β heterodimer but is retained either in the presence of an A-type lattice with a B-type "seam" or in a B-type lattice with an A-type "seam." These categories therefore include all microtubule lattices, with and without seams, irrespective of the protofilament number.

These results have some bearing on the significance of the existence of microtubules with different lattice types. As discussed above, for any lattice other than the A-type with an odd number of protofilaments, a structural seam must be present. The fact that microtubules with n in the range 12 to 16 are found to coexist in self-assembled microtubule populations, with $n = 13$ and 14 most common, implies that a protofilament "seam" cannot be a source of unusual instability in the microtubule structure. This suggests that the heterologous $\bar{3}$-start α-β/β-α interactions and the homologous $\bar{3}$-start α-α/β-β interactions are probably similar in free energy. Similar conclusions appear likely for interactions in the 5- and $\bar{8}$-start directions. This, in turn, increases the likelihood that microtubule lattices may include both types of interactions (cf. the "mixed" A/B lattices originally proposed by McEwen and Edelstein) (23). Thus, whereas a seeding structure could well impose a given lattice type by microtubule growth with fidelity (19, 49), the energetic cost of a lattice defect, as either a change of type (A/B) or even a change in protofilament number (as rarely seen) (21), need not be prohibitively expensive in energy terms.

The property of dynamic instability appears to be unique to the microtubule structure. However, the simulations suggest that it does not seem to be necessarily correlated with a single, perfectly regular structure for the microtubule lattice. The origin of the phenomenon appears to reside partly in the apparent high affinity of Tu-GTP for the microtubule end and in the stability of the microtubule in the growing state. In addition, the overall microtubule lattice structure is important. Thus, as suggested previously for the helically symmetric 13-A lattice (7), the $\bar{3}$-start helix, dictated by the details of protein-protein contact at the level of the tubulin monomer, determines that the microtubule end has a number of relatively short "runs" of symmetry-related molecules (see, for example, protofilaments 6 to 11 in Fig. 1 *A*). The general treatment of lattice energies presented here shows how these molecules can interact with a degree of cooperativity. Irrespective of the exact nature of the $\bar{3}$-start contacts, and hence including all types of microtubule lattice, this cooperativity gives rise to the two-state growing and shortening behavior and determines the extent of the concentration range about C_c over which microtubules exhibit dynamic instability.

The effect of dynamic instability is to confer specialized properties on the microtubule structure formed by a relatively simple GTP-dependent protein assembly process. The microtubule, in the presence of a suitable concentration of Tu-GTP, is apparently physically stable, although it is effectively composed entirely of Tu-GDP. It is more appropriate to describe it as a metastable structure, stabilized by the kinetic event of Tu-GTP addition. When the stabilizing effect of Tu-GTP addition is lost, the microtubule undergoes rapid disassembly by endwise loss of Tu-GDP. This metastability provides a polar structure that is evidently physically stable and relatively rigid and which is used in cellular systems to establish or stabilize the directionality of cytoplasmic structures and processes. At the same time, the physical properties of the lattice allow microtubules to be rapidly reorganized under the influence of appropriate factors.

Factors controlling microtubule dynamic instability

It appears likely that the phenomenon of microtubule dynamic instability is influenced by a variety of factors, especially for microtubules within the cytoplasmic milieu. The simulations described here have shown that the basic properties of microtubule dynamic instability can derive from purely physical and kinetic effects, that is, the transition behavior is an intrinsic property for an individual microtubule in the presence of a constant concentration of Tu-GTP within a given range and under a given set of solution conditions.

It is therefore instructive to consider how simple changes in these conditions could affect the dynamic behavior of microtubules.

The treatment described above indicates that a principal factor controlling dynamic instability is the effective concentration of free Tu-GTP. In the simulations, this concentration, plus the bimolecular rate constant, determines the rate of addition of Tu-GTP and hence the probability of an addition event relative to a dissociation event. However, this concentration factor has to be considered in relation to the value of C_c, the critical concentration for microtubule assembly under the given conditions. In fact, it would be more appropriate to consider the dependence of transition frequencies on the normalized concentration, γ (= [Tu-GTP]/C_c). Studies over many years have shown that the parameter C_c is itself affected by the type of buffer ion and its concentration, solution pH, temperature, the presence of stabilizing agents (glycerol, etc.), the presence of microtubule-associated proteins (MAPs), and the presence of agents that bind to tubulin and affect assembly properties, including nucleotides (e.g., GDP), drugs (e.g., colchicine), and ions (e.g., Ca^{2+}) (see Ref. 50 and references therein).

Many of these factors can have complicated and multiple interrelated effects; for example, high [Mg^{2+}] can increase the C_c but at the same time stabilize tubulin-GDP as oligomers, hence inhibiting the exchange reaction with GTP that regenerates tubulin-GTP. In the simplest case, for a fixed value of [Tu-GTP], a factor that selectively increases the C_c will decrease γ, and the balance of dynamic processes is shifted to show greater frequency of G→S transitions (so-called catastrophe). The effectively inverse relationship between the dependence on [Tu-GTP] (or γ) of G→S and S→G transition frequencies in the concentration range about C_c, where dynamics are most readily observed, means that the corresponding effect of the same factor on the S→G transitions could be relatively small. Thus the factor appears to be affecting the G→S or "catastrophe" frequency selectively. Conversely, a factor that selectively decreases the value of C_c will increase γ and show a more marked effect on the S→G or "rescue" frequency. In either case, effects of the given factor on the characteristic rates of the growth phase and shortening phase may well be negligibly small since [Tu-GTP] remains constant. (The modeling suggests a second-order effect might be expected owing to some dependence of k_{obs}(+T) and k_{obs}(−D) on [Tu-GTP], due to the changes in the proportions of "mixed ends" containing Tu-GTP and Tu-GDP in the region of the C_c (see Ref. 14).

Several reports have shown significant effects on the dynamic properties of individual microtubules by agents added to solutions containing microtubules showing dynamic transitions. O'Brien et al. (39) showed effects of Mg^{2+} on the dynamic instability of individual microtubules. This correlates with the observations of Gal et al. (40) of fast disassembly of bulk microtubules induced by Mg^{2+} and Ca^{2+}. More recently, Simon et al. (51) noted that different buffer ions (4-(2-hydroxyethyl)-1-piperazineethanesulfonic acid, 1,4-piperazinediethanesulfonic acid) produced characteristic differences in growth rates and transition behavior for microtubules of sea urchin tubulin assembled in vitro. Likewise, the presence of MAPs can have a marked effect on dynamics (3, 33). In fact, the addition of MAPs generally reduces the value of C_c, suggesting a lower probability for the G→S transitions. However, under these conditions, the mechanisms and kinetics of microtubule elongation and disassembly are likely to differ significantly from the situation with pure Tu-GTP, as shown for microtubule protein preparations (52).

The simulations suggest that one factor that clearly needs careful control in experiments where GTP hydrolysis occurs is the level of GDP and hence Tu-GDP. Even within the limits of the mechanism involving simple addition and dissociation of tubulin monomers at the microtubule end, pronounced kinetic effects are expected, even in the presence of a low molar ratio of Tu-GDP/Tu-GTP (see Fig. 9). These effects will in general be toward destabilization of the microtubule, increase of C_c, and increased frequency of G→S and S→G transitions. Furthermore, when Tu-GDP is present under conditions that promote the formation of oligomeric tubulin species, the growth and shortening of microtubules may be affected in an unpredictable way owing to a change in mechanism via the involvement of oligomers in competing reactions.

Likewise, at the macroscopic level, the number and hence length of microtubules will be critically dependent on the number of initiation sites involved. A significant increase in this number, when assembly is well advanced or close to steady state, will increase the microtubule number concentration and hence decrease the mean length. The onset of this process may easily resemble an effectively concerted transition from growth to shortening, without the involvement of any factor acting on the microtubules themselves (14, 53). The net result would be a significant and progressive shift in the length distribution profile to lower values. Thus even under the relatively well-controlled conditions of in vitro experimentation, small changes in solution conditions may produce unexpected dynamic behavior in a population of microtubules.

A number of studies have shown that microtubule dynamic instability occurs in the cytoplasm of live cells at interphase (4, 54–56) and in mitosis (57). The characteristic transition behavior in interphase appears more complicated than in vitro, with less regular growth rates. In the cytoplasm, it is difficult to assess even the effective concentration of tubulin, and there is a multiplicity of additional factors which, as noted above, may change fundamental parameters such as the value of the C_c, as well as affecting the intrinsic mechanisms of microtubule assembly.

Several studies have sought to clarify this situation, using assays of the dynamics of microtubules nucleated from centrosomes in cytoplasmic extracts. The activity of cell-cycle-dependent enzymic factors, notably $p34^{cdc2}$ kinase, plus cyclin B, have been implicated in increasing the G→S transition rate, as judged by direct observations, and measurements of length distributions of microtubule populations

initiated on centrosomes (58–60). In this context, it is interesting that okadaic acid, an inhibitor of phosphatases that prolongs mitosis in sea urchin eggs, has been reported to induce short, dynamic microtubules in sea urchin extracts (61), whereas 6-dimethylaminopurine, an inhibitor of $p34^{cdc2}$ kinase, apparently supports long microtubules (58). These enzymic factors may act by modulating the nucleation capacity of centrosomes in such extracts, in addition to possible effects on microtubule-associated proteins. Clearly it will be important for mechanistic reasons to know how close is the system to the value of C_c which characterizes a steady state of assembly and how far observed changes in growth rates and transition frequencies represent a transient response under non-steady-state conditions to a change in microtubule number induced by the application of the agent in question. Recent studies have shown the high dynamic activity of sea urchin egg tubulin in cytoplasmic extracts, compared with the same protein in standard buffers (51). Individual microtubules showed enhanced growth rates and apparently greater G→S transition rates, consistent with the involvement of unknown cytoplasmic factors in some regulatory function. For the present it is significant that additional factors can modulate the dynamic properties of microtubules in the direction of stabilization or destabilization, effects that could be of considerable value in regulation processes in vivo. These results indicate that the full description of the dynamics of a microtubule population in vivo involves a multiplicity of factors, but appreciation of the intrinsic physical properties of the microtubule lattice itself, including the nucleotide-dependent metastability as described above, remains central to the phenomenon.

The biological function of microtubule dynamic instability appears to be in ensuring such properties as the correct location of microtubules in mitosis, conferring a dynamic structure to an extended microtubule bundle, as in neurons, and allowing an exploratory feature of microtubules in neurite outgrowth (62–64). Given the critical biological role of these processes, it is quite remarkable that the unique property of the dynamic instability of microtubule structure can persist, given the possibilities of significant variation and imperfection in the microtubule lattice geometry.

We thank Jose-Manuel Andreu, Yves Engelborghs, Martyn Symmons, and Andre Vandecandelaere for constructive comments.
This work is supported in part by EC twinning grant 902/00203.
A demonstration copy of the simulation program will be available from the authors.

REFERENCES

1. Mitchison, T., and M. W. Kirschner. 1984. Microtubule assembly nucleated by isolated centrosomes. *Nature.* 312:232–237.
2. Mitchison, T., and M. W. Kirschner. 1984. Dynamic instability of microtubule growth. *Nature.* 312:237–242.
3. Horio, T., and H. Hotani. 1986. Visualisation of the dynamic instability of individual microtubules by dark-field microscopy. *Nature.* 321: 605–607.
4. Cassimeris, L. U., N. K. Pryer, and E. D. Salmon. 1988. Real-time observations of microtubule dynamic instability in living cells. *J. Cell Biol.* 107:2223–2231.
5. Walker, R. A., E. T. O'Brien, N. K. Pryer, M. Soboeiro, W. A. Voter, H. P. Erickson, and E. D. Salmon. 1988. Dynamic instability of individual, MAP-free microtubules analysed by video light microscopy: rate constants and transition frequencies. *J. Cell Biol.* 107:1437–1448.
6. Carlier, M-F. 1989. Role of nucleotide hydrolysis in the dynamics of actin filaments and microtubules. *Int. Rev. Cytol.* 115:139–170.
7. Bayley, P. M. 1990. What makes microtubules dynamic? *J. Cell Sci.* 95:329–334.
8. Engelborghs, Y. 1990. Dynamic aspects of microtubule assembly. *In* Microtubule Proteins. J. Avila, editor. CRC Press, Boca Raton, FL. 1–35.
9. Mandelkow, E-M., and E. Mandelkow. 1992. Microtubule oscillations. *Cell Motil. Cytoskeleton.* 22:235–1244.
10. Bayley, P. M., and S. R. Martin. 1992. Microtubule dynamic instability: basic mechanisms and numerical modelling by computer simulation. *Comments Theor. Biol.* 2:403–427.
11. Caplow, M. 1992. Microtubule dynamics. *Curr. Opinion Cell Biol.* 4:58–65.
12. Erickson, H. P., and E. T. O'Brien. 1992. Microtubule dynamic instability and GTP hydrolysis. *Annu. Rev. Biophys. Biomol. Struct.* 21: 145–166.
13. Bayley, P. M., M. J. Schilstra, and S. R. Martin. 1989. A lateral cap model for microtubule dynamic instability. *FEBS Lett.* 259:181–184.
14. Bayley, P. M., M. J. Schilstra, and S. R. Martin. 1990. Microtubule dynamic instability: numerical simulation of microtubule transition properties using a lateral cap model. *J. Cell Sci.* 95:33–48.
15. Bayley, P. M., S. R. Martin, and K. K. Sharma. 1991. Dynamic microtubules: experimental observation and computer simulation of polar microtubule behaviour with lateral cap model mechanisms. *Am. Inst. Phys. Conf. Proc.* 226:187–199.
16. Martin, S. R., M. J. Schilstra, and P. M. Bayley. 1991. Opposite-end behaviour of dynamic microtubules. *Biochim. Biophys. Acta.* 1073: 555–561.
17. Chen, Y., and T. L. Hill. 1985. Monte Carlo study of the GTP cap in a five-start helix model of a microtubule. *Proc. Natl. Acad. Sci. USA.* 82:1131–1135.
18. Allen, C., and G. G. Borisy. 1974. Structural polarity and directional growth of microtubules of *Chlamydomonas* flagella. *J. Mol. Biol.* 90: 381–402.
19. Evans, T., T. Mitchison, and M. W. Kirschner. 1985. Influence of the centrosome on the structure of nucleated microtubules. *J. Cell Biol.* 100:1185–1191.
20. Wade, R. H., D. Chrétien, and D. Job. 1990. Characterisation of microtubule protofilament numbers. How does the surface lattice accommodate? *J. Mol. Biol.* 212:775–786.
21. Chrétien, D., F. Metoz, F. Verde, E. Karsenti, and R. H. Wade. 1992. Lattice defects in microtubules: protofilament numbers vary within individual microtubules. *J. Cell Biol.* 117:1031–1040.
22. Amos, L. A. 1979. Structure of microtubules. *In* Microtubules. K. Roberts and J. S. Hyams, editors. Academic Press, London. 1–64.
23. McEwen, B., and S. J. Edelstein. 1977. Evidence for a mixed lattice in microtubules reassembled in vitro. J. Mol. Biol. 139:123–145.
24. Mandelkow, E-M., R. Schultheiss, R. Rapp, M. Muller, and E. Mandelkow. 1986. On the surface lattice of microtubules: helix starts, protofilament number, seam and handedness. *J. Cell Biol.* 102:1067–1073.
25. Song, Y-H., and E. Mandelkow. 1993. Recombinant kinesin motor domain binds to β-tubulin and decorates microtubules with a B surface lattice. *Proc. Natl. Acad. Sci. USA.* 90:1671–1675.
26. Erickson, H. P. 1989. Co-operativity in protein-protein association. The structure and stability of the actin filament. *J. Mol. Biol.* 206:465–474.
27. David-Pfeuty, T., J. Laporte, and D. Pantaloni. 1978. GTPase activity at the ends of microtubules. *Nature.* 272:282–284.
28. Kleutsch, B., and E. Frehland. 1991. Monte Carlo simulations of voltage fluctuations in biological membranes in the case of small numbers of transport units. *Eur. Biophys. J.* 19:203–211.
29. Howard, W. D., and S. N. Timasheff. 1986. GDP state of tubulin: stabilization of double rings. *Biochemistry.* 25:8292–8300.
30. Mandelkow, E., E-M. Mandelkow, and J. Bordas. 1983. Structure of tubulin rings studied by X-ray scattering using synchrotron radiation.

J. Mol. Biol. 167:179–196.

31. Mandelkow, E-M., E. Mandelkow, and R. A. Milligan. 1991. Microtubule dynamics and microtubule caps: a time-resolved cryo-electron microscopy study. *J. Cell Biol.* 114:977–991.
32. Dye, R. B., P. F. Flicker, D. Y. Lien, and R. C. Williams. 1992. End-stabilized microtubules observed in vitro: stability, subunit interchange, and breakage. *Cell Motil. Cytoskeleton.* 21:171–186.
33. Pryer, N. K., R. A. Walker, V. P. Skeen, B. D. Bourns, M. F. Soboeiro, and E. D. Salmon. 1992. Brain microtubule-associated proteins modulate microtubule dynamic instability in vitro. Real-time observations using video microscopy. *J. Cell Sci.* 103:965–976.
34. Mandelkow, E-M., G. Lange, A. Jagla, U. Spann, and E. Mandelkow. 1988. Dynamics of the microtubule oscillator: role of nucleotides and tubulin-MAP interactions. *EMBO J.* 7:357–365.
35. Walker, R. A., N. K. Pryer, and E. D. Salmon. 1991. Dilution of individual microtubules observed in real time in vitro: evidence that the cap size is small and independent of elongation rate. *J. Cell Biol.* 114: 73–81.
36. Caplow, M., and J. Shanks. 1990. Mechanism of the microtubule GTPase reaction. *J. Biol. Chem.* 265:8935–8941.
37. Symmons, M. F., S. R. Martin, and P. M. Bayley. 1991. Biochemical studies of microtubule dynamic instability. *J. Cell Biol.* 115:37a.
38. Simon, J. R., and E. D. Salmon. 1990. The structure of microtubule ends during the elongation and shortening phases of dynamic instability examined by negative-stain electron microscopy. *J. Cell Sci.* 96:571–582.
39. O'Brien, E. T., E. D. Salmon, R. A. Walker, and H. P. Erickson. 1990. Effects of magnesium on the dynamic instability of individual microtubules. *Biochemistry.* 29:6648–6656.
40. Gal, V., S. R. Martin, and P. M. Bayley. 1988. Fast disassembly of microtubules induced by Mg^{2+} or Ca^{2+}. *Biochem. Biophys. Res. Commun.* 155:1464–1470.
41. Gildersleeve, R. F., A. R. Cross, R. E. Cullen, A. P. Fagen, and R. C. Williams. 1992. Microtubules grow and shorten at intrinsically variable rates. *J. Biol. Chem.* 267:7995–8006.
42. Carlier, M-F., T. L. Hill, and Y-D. Chen. 1984. Interference of GTP hydrolysis in the mechanism of microtubule assembly. *Proc. Natl. Acad. Sci. USA.* 81:771–775.
43. Martin, S. R., and P. M. Bayley. 1992. Simulation of tubulin loss from the microtubule wall. *Mol. Biol. Cell.* 3:166a.
44. Schilstra, M. J., S. R. Martin, and P. M. Bayley. 1989. The effect of podophyllotoxin on microtubule dynamics. *J. Biol. Chem.* 264:8827–8834.
45. Bayley, P. M., and S. R. Martin. 1991. Microtubule dynamic instability: some possible physical mechanisms and their implications. *Biochem. Soc. Trans.* 19:1023–1028.
46. Skoufias, D. A., and Wilson, L. 1992. Mechanism of inhibition of microtubule polymerization by colchicine: inhibitory potencies of unliganded colchicine and tubulin-colchicine complexes. *Biochemistry.* 31: 738–746.
47. Jordan, M. A., R. J. Toso, D. Thrower, H. P. Miller, and L. Wilson. 1991. Inhibition of microtubule dynamics *in vitro* and *in vivo* by nocodazole. *J. Cell Biol.* 115:36a.
48. Toso, R. J., M. A. Jordan, and L. Wilson. 1991. Colchicine and vinblastine suppress dynamic instability of individual microtubules. *J. Cell Biol.* 115:36a.
49. Scheele, R. B., L. G. Bergen, and G. G. Borisy. 1982. Control of structural fidelity of microtubules by initiation sites. *J. Mol. Biol.* 154:485–500.
50. Schilstra, M. J., P. M. Bayley, and S. R. Martin. 1991. The effect of solution composition on microtubule dynamic instability. *Biochem. J.* 277:839–847.
51. Simon, J. R., S. F. Parsons, and E. D. Salmon. 1992. Buffer conditions and non-tubulin factors critically affect the microtubule dynamic instability of sea urchin egg tubulin. *Cell Motil. Cytoskeleton.* 21:1–14.
52. Bayley, P. M., F. M. M. Butler, D. C. Clark, E. J. Manser, and S. R. Martin. 1985. The assembly of microtubule protein in vitro. The kinetic role in microtubule elongation of oligomeric fragments containing microtubule-associated proteins. *Biochem. J.* 227:439–455.
53. Obermann, J., E-M. Mandelkow, G. Lange, and E. Mandelkow. 1990. Microtubule oscillations. Role of nucleation and microtubule number concentration. *J. Biol. Chem.* 265:4382–4388.
54. Cassimeris, L. U., R. A. Walker, N. K. Pryer, and E. D. Salmon. 1987. Dynamic instability of microtubule. *Bioessays.* 7:149–154.
55. Sammak, P. J., and G. G. Borisy. 1988. Direct observation of microtubule dynamics in living cells. *Nature.* 332:724–726.
56. Schulze, E., and M. W. Kirschner. 1988. New features of microtubule behaviour observed in vivo. *Nature.* 334:356–359.
57. Hayden, J. H., S. S. Bowser, and C. L. Rieder. 1990. Kinetochores capture astral microtubules during chromosome attachment to the mitotic spindle: direct visualisation in live newt lung cells. *J. Cell Biol.* 111:1039–1046.
58. Verde, F., J. C. Labbe, M. Doree, and E. Karsenti. 1990. Regulation of microtubule dynamics by cdc2 protein kinase in cell extracts. *Nature.* 343:233–238.
59. Verde, F., M. Dogterom, E. Stelzer, E. Karsenti, and S. Leibler. 1992. Control of microtubule dynamics and length by cyclin A and cyclin B dependent kinase in *Xenopus* egg. *J. Cell Biol.* 118:1098–1108.
60. Belmont, L. D., A. A. Hyman, K. E. Sawin, and T. J. Mitchison. 1990. Real-time visualisation of cell cycle dependent changes in microtubule dynamics in cytoplasmic extracts. *Cell.* 62:579–589.
61. Gliksman, N. R., S. F. Parsons, and E. D. Salmon. 1992. Okadaic acid induces interphase to mitotic-like microtubule dynamic instability by inactivating rescue. *J. Cell Biol.* 119:1271–1276.
62. Kirschner, M. W., and T. Mitchison. 1986. Beyond self-assembly: from microtubules to morphogenesis. *Cell.* 45:329–342.
63. Kirschner, M. W. 1988. Biological implications of microtubule dynamics. *Harvey Lect.* 83:1–20.
64. Mitchison, T., and M. W. Kirschner. 1988. Cytoskeletal dynamics and nerve growth. *Neuron.* 1:761–772.